

## RESEARCH ARTICLE

# The butyrophilin 1a1 knockout mouse revisited: Ablation of *Btn1a1* leads to concurrent cell death and renewal in the mammary epithelium during lactation

Jaekwang Jeong<sup>1</sup> | Anil K. G. Kadegowda<sup>1</sup> | Thomas J. Meyer<sup>2,3</sup> | Lisa M. Jenkins<sup>4</sup> | Jerry C. Dinan<sup>4</sup> | John J. Wysolmerski<sup>5</sup> | Roberto Weigert<sup>6</sup> | Ian H. Mather<sup>1,6</sup> 

<sup>1</sup>Department of Animal and Avian Sciences, University of Maryland, College Park, Maryland, USA

<sup>2</sup>CCR Collaborative Bioinformatics Resource, National Cancer Institute, National Institutes of Health, Bethesda, Maryland, USA

<sup>3</sup>Advanced Biomedical Computational Science, Frederick National Laboratory for Cancer Research, Frederick, Maryland, USA

<sup>4</sup>Laboratory of Cell Biology, National Cancer Institute, National Institutes of Health, Bethesda, Maryland, USA

<sup>5</sup>Department of Internal Medicine, Yale University School of Medicine, New Haven, Connecticut, USA

<sup>6</sup>Laboratory of Cellular and Molecular Biology, Center for Cancer Research, National Cancer Institute, National Institutes of Health, Bethesda, Maryland, USA

## Correspondence

Ian H. Mather, Department of Animal and Avian Sciences, University of Maryland, College Park, MD 20742, USA.

Email: imather@umd.edu

## Present address

Jaekwang Jeong, Section of Endocrinology and Metabolism, Department of Internal Medicine, Yale University School of Medicine, New Haven, Connecticut 06520, USA

Anil K. G. Kadegowda, Department of Animal Sciences, University of Agricultural Sciences Dharwad, Hubli, Karnataka 580005, India

## Funding information

NIH, Grant/Award Number: R01HD06248, R01HD100468 and R01HD048588-01A1; U.S. Department of Agriculture, Grant/Award Number: NRI 0003264 and 2005-04637

## Abstract

Butyrophilin 1A1 (BTN1A1) is implicated in the secretion of lipid droplets from mammary epithelial cells as a membrane receptor, which forms a secretion complex with the redox enzyme, xanthine oxidoreductase (XDH). The first evidence that BTN1A1 functions in this process was the generation of *Btn1a1*<sup>-/-</sup> mouse lines, in which lipid secretion was disrupted and large unstable droplets were released into alveolar spaces with fragmented surface membranes. We have revisited one of these mutant mouse lines using RNAseq and proteomic analysis to assess the consequences of ablating the *Btn1a1* gene on the expression of other genes and proteins. Disruption of intact *Btn1a1* protein expression led to a large build-up of Xdh in the cytoplasm, induction of acute phase response genes and Lif-activation of Stat3 phosphorylation. At peak lactation, approx. 10% of the cells were dying, as assessed by TUNEL-analysis of nuclear DNA. Possible cell death pathways included expression of caspase 8 and activated caspase 3, autophagy, Slc5a8-mediated inactivation of survivin (Birc5), and pStat3-mediated lysosomal lysis, the latter of which is the principal death route in involuting wild type cells. Milk secretion was prolonged by renewal of the secretory epithelium, as evidenced by the upregulation of Ki67 in approx. 10% of cell nuclei and expression of cyclins and Fos/Jun. These data highlight the plasticity of the

**Abbreviations:** HRP, horse radish peroxidase; LD, lipid droplet; PBS, phosphate-buffered saline; PNS, post-nuclear supernatant; TBS, Tris-buffered saline; TH, total homogenate.

This is an open access article under the terms of the Creative Commons Attribution-NonCommercial License, which permits use, distribution and reproduction in any medium, provided the original work is properly cited and is not used for commercial purposes.

©2021 The Authors *FASEB BioAdvances* published by The Federation of American Societies for Experimental Biology

mammary epithelium and the importance of functional BTN1A1 expression for maintenance of terminally differentiated secretory cells and optimal milk production throughout lactation.

#### KEYWORDS

apoptosis, butyrophilin 1a1, cell death, cell renewal, milk-lipid secretion, xanthine oxidoreductase

## 1 | INTRODUCTION

Butyrophilin 1A1 (BTN1A1) was first identified as an integral membrane protein associated with lipid droplets in the milk of many species.<sup>1–3</sup> Later analysis showed that the gene, *BTN1A1* is one of at least 13 *BTN1A1*-like genes within and outside of the human MHC or its functional equivalent in other species.<sup>4</sup> All of the gene products are members of the immunoglobulin superfamily with a variable number of immunoglobulin-like folds in the exoplasmic domain, a single transmembrane anchor and (usually) an extensive cytoplasmic region, which includes a PRY/SPRY/B 30.2 domain.<sup>4,5</sup> This latter domain functions as a module for binding to other proteins and molecules<sup>6–8</sup> and is encoded in many genes from teleost fish to humans.<sup>9,10</sup> Recent and expanding research has revealed multiple immune functions for the BTNs, including both inhibitory and stimulatory effects on T-cell differentiation, activation, and antigen sensing.<sup>4,11</sup>

The eponymous BTN1A1 protein is highly expressed on the apical plasma membrane of mammary secretory cells during lactation and is postulated to play a key role in the secretion of lipid droplets (LDs) together with the soluble redox enzyme, xanthine oxidoreductase (XDH). LDs are transported from sites of synthesis to the cell apex and bud from the apical surface enveloped with cellular membranes.<sup>12</sup> The first *functional* evidence that Btn1a1 plays a role in this process was the analysis of two mutant mouse lines, *Btn1a1*<sup>−/−</sup> KO1 and KO2, in which *Btn1a1* was either disrupted or presumed to be ablated, respectively.<sup>13</sup> LD secretion was severely impacted in both mouse lines, unstable droplets emerged from the cell with disrupted membrane envelopes and the secreted lipid fused *en masse* in luminal spaces. Litter weights were 60%–80% of wild type levels and up to half of the pups died before weaning. Subsequently, Xdh was shown to bind to the C-terminal region of the PRY/SPRY/B30.2 domain in the cytoplasmic tail of Btn1a1.<sup>7</sup> These observations supported a theoretical model for LD secretion<sup>14</sup> in which Btn1a1 in the plasma membrane and Xdh in the cytoplasm, form a docking complex with other proteins that ensures close interaction between the surface of the droplets and the cytoplasmic face of the plasma membrane. In agreement

with this model, analysis of a conditional knockout of *Xdh* has shown that Xdh is required to recruit Btn1a1 into the docking complex and that in the absence of Xdh large LDs accumulate in a similar manner to the Btn1a1 null mouse.<sup>15</sup> Such functional Btn1a1-Xdh interactions are also compatible with additional mutant mouse lines impacting either Btn1a1 and/or Xdh expression during lactation.<sup>16–18</sup>

To probe the function of Btn1a1 in more detail, we undertook an RNAseq and proteomic analysis of the *Btn1a1*<sup>−/−</sup> KO2 mouse line that has revealed a more complex phenotype than originally supposed. Disruption of LD secretion precipitated significant cell death, such that lactation was only maintained by compensatory cell replacement.

## 2 | MATERIALS AND METHODS

### 2.1 | Materials

Aprotinin, *N*<sup>α</sup>-*p*-tosyl-L-lysine chloromethyl ketone, *N*<sup>α</sup>-*p*-tosyl-L-phenylalanine chloromethyl ketone, tribromethanol (Avertin), digitonin, bovine serum albumin (BSA), Roche cOmplete<sup>TM</sup> proteinase inhibitor tablets and a Lipid Peroxidation Assay kit were obtained from Sigma (St. Louis, MO). ECL western blot detection reagents were either from Amersham Biosciences/GE Healthcare (Pittsburgh, PA) or Cell Signaling Technology (Danvers, MA). Horseradish peroxidase (HRP)-conjugated goat anti-rabbit secondary antibody (blotting grade), Triton X-100, Tween 20, SDS, acrylamide, bisacrylamide, electrophoretic molecular weight standards, and IQ<sup>TM</sup> SYBR<sup>®</sup> Green supermix were from Bio-Rad (Hercules, CA). Ketamine was from Putney (Portland, ME) and xylazine from MWI (Boise, ID). DNA polymerases, dNTPs, and trypsin were from Promega (Madison, WI), and phenylmethylsulfonyl fluoride was obtained from Calbiochem (Gibbstown, NJ). TRIzol reagent, goat anti-(rabbit IgG)-FITC, goat anti-(rabbit IgG)-AlexaFluor<sub>488</sub> and AlexaFluor<sub>568</sub>, goat anti-(rat-IgG)-AlexaFluor<sub>555</sub>, WGA-AlexaFluor<sub>633</sub> conjugate, UltraPure<sup>TM</sup> LMP agarose, and Dulbecco's phosphate-buffered saline (DPBS) were from Invitrogen (Carlsbad, CA). O.C.T compound was from Sakura Finetek U.S.A

(Dublin, OH) and Fluoromount G from Electron Microscopy Sciences (Hatfield, PA). Vectashield® and the ABC Vector stain kit were from Vector Laboratories (Burlingame, CA). The In Situ Cell Death Detection kit was from Roche (Florence, SC). Direct-zol RNA Miniprep Plus kits were from Zymo Research Corp. (Irvine, CA) and immunoblotting kits for detection of oxidative damage to proteins from Cell BioLabs Inc (San Diego, CA). An RNeasy cleanup kit was from Qiagen (Valencia, CA) and MS-grade trypsin was from Thermo (Waltham, MA). All other reagents, including solvents for LC-MS, were from Fisher. Details of in-house and commercial primary antibodies used for immunoblotting and immunohistochemistry are summarized in Table S1.

## 2.2 | Animals

C57Bl/6 mice were purchased from Charles River Inc. (Wilmington, MA). The *Btn* null strain (*Btn1a1*<sup>-/-</sup>) was the *Btn1a1*<sup>-/-</sup> KO2 strain of Ogg et al.,<sup>13</sup> and the *Xdh* null strain (*Xdh*<sup>-/-</sup>) was a gift from Dr. Toren Finkel (National Heart, Blood and Lung Institute, NIH, Bethesda, MD).<sup>19</sup> Both mutant strains were derived from 129 ES cells and maintained on a C57Bl/6 background. Mice were either fed Formulab Diet 5008 (PMI Nutrition, Richmond, IN), or NIH 31 Open Formula Diet 7017 (Envigo, Madison, WI) and supplied with water ad libitum.

The wild type mouse strains were harem bred one male to two females per cage and both mutant mouse strains were separately maintained by mating single-pair heterozygotes. For experimental purposes, wild type, heterozygote, and knockout mice were compared by breeding heterozygotes from within the same backcrossed generation. To produce the single and double mutant mice compared in Figure 1, *Btn1a1*<sup>+/-</sup>*Xdh*<sup>+/-</sup> mice were crossed with each other to generate *Btn1a1*<sup>+/+</sup>*Xdh*<sup>+/+</sup>, *Btn1a1*<sup>+/-</sup>*Xdh*<sup>+/+</sup>, *Btn1a1*<sup>+/-</sup>*Xdh*<sup>+/-</sup>, *Btn1a1*<sup>+/+</sup>*Xdh*<sup>+/-</sup>, *Btn1a1*<sup>-/-</sup>*Xdh*<sup>+/+</sup>, and *Btn1a1*<sup>-/-</sup>*Xdh*<sup>+/-</sup>. Note that the lactation phenotype of *Xdh*<sup>-/-</sup> mice could not be analyzed because null animals die of severe kidney dysplasia within the first month post-partum.<sup>19</sup>

In all cases, the first full day after parturition was counted as day 1 and litters were adjusted to six pups per mother. For a summary of animal usage see Table S2. All animal procedures were approved by the Institutional Animal Care and Use Committees of the University of Maryland, College Park and the NIH and were in compliance with the US National Research Council's Guide for the Care and Use of Laboratory Animals, the US Public Health Service's Policy on Humane Care and Use of Laboratory Animals and the Guide for the Care and Use of Laboratory Animals.

## 2.3 | Preparation of tissue fractions

Mice were briefly treated with isoflurane 3.0%–3.5% followed by an intraperitoneal injection of a mixture of xylozine and ketamine (20 and 100 mg/kg body weight, respectively) to induce a deep plane of anesthesia through-out surgery. All of the mammary glands were excised and weighed and tissue pieces suspended in three volumes of Tris-buffered saline (TBS; 10 mM Tris-HCl, 140 mM NaCl, pH 7.2) containing proteinase inhibitors [0.1 mM phenylmethylsulfonyl fluoride, 0.1 mM N<sup>α</sup>-p-tosyl-L-lysine chloromethyl ketone, 0.1 mM N<sup>α</sup>-p-tosyl-L-phenylalanine chloromethyl ketone, aprotinin (8.2 IU/ml), and 1 mM ε-aminocaproic acid] per g of tissue. For homogenates used for immunoblots this mixture was supplemented with one tablet of proteinase inhibitor (Roche cOmplete™) per 10 ml of TBS. The tissue was minced finely and homogenized on ice using a Polytron homogenizer by giving five pulses of 10 s each at a speed setting of six. Total homogenates (THs) were centrifuged at 500 g<sub>av</sub> for 5 min at 4°C to obtain sediments and supernatants, operationally called the “nuclear fraction” and “post-nuclear supernatants (PNSs)”, respectively. Most of the immunoblots discussed were developed using TH fractions as indicated in Figure legends. In some cases, the PNSs were further centrifuged at 100,000 g<sub>av</sub> at 4°C for 1h to prepare “microsomal membrane” and “post-microsomal supernatant” fractions. Microsomal membrane fractions were resuspended in a minimal volume of RIPA buffer [1% (v/v) NP-40, 0.5% (w/v) sodium deoxycholate, 0.1% (w/v) SDS, 10 mM Tris, and 150 mM NaCl, pH 7.4] containing the above proteinase inhibitors and stored at -80°C, together with the nuclear, TH, PNS, and post-microsomal supernatant fractions.

## 2.4 | Electrophoresis and immunoblot

Proteins were separated by SDS-polyacrylamide gel electrophoresis and electrophoretically transferred to nitrocellulose paper or polyvinylidene fluoride (PVDF) membrane following standard procedures.<sup>20,21</sup> Molecular weight markers were always included for reference and comprised a mixture of recombinant proteins of M<sub>r</sub> 10 to 250 x 10<sup>3</sup> (Precision Plus protein standards, Bio-Rad). Immunoblots were stained with Ponceau S to assess loading efficiency and then in most instances blocked overnight with 3% (w/v) gelatin/TBS containing 0.1% (v/v) Tween 20. Powdered milk [5.0% (w/v)] or BSA [5.0% (w/v)], in either PBS or TBS supplemented with Tween 20 was only used for the development of commercial antibodies to Stat3/pStat3, Stat5/pStat5, Cathepsin B, dinitrophenol, and nitrotyrosine as directed by the respective manufacturers. The concentrations of

antibodies used for each blot (Table S1) are summarized in the figure legends. Immunoblots were developed by enhanced chemiluminescence using SignalFire™ ECL reagent from Cell Signaling Technology and recorded with a ChemiDoc Imaging System (Bio-Rad). Relative amounts of each antigen were estimated by densitometry using QuantityOne software (Bio-Rad) under non-saturating conditions and corrected for well-loading variations by reference to the combined density of all Ponceau S stained proteins in each lane. Relative concentrations of each protein were normalized to an appropriate reference antigen set to 100% on replicate blots as indicated in the figure legends.

## 2.5 | Immunohistochemistry of unfixed tissue

Mammary tissue was flash-frozen in isopentane held in liquid nitrogen, sectioned and thawed to room temperature on microscope slides. Unfixed sections, were either treated with PBS alone (control), or 20  $\mu$ M digitonin in PBS (test) for 10 min. Xdh was detected in the tissue with a 1- to 100-fold dilution of rabbit anti-peptide antibody to mouse Xdh,<sup>7</sup> followed by a 1- to 500-fold dilution of goat anti-(rabbit IgG)-FITC. In addition, nuclei were stained with DAPI, LDs with Nile red (1: 1,000 dilution) and apical surfaces with WGA-AlexaFluor<sub>633</sub> (1:500 dilution). Sections were sequentially scanned with a Leica SP5X confocal laser scanning microscope equipped with diode and white-light lasers for DAPI (excitation 405 nm, emission 416–439 nm), FITC (excitation 488 nm, emission 505–524 nm), Nile red (excitation 550 nm, emission 583–599 nm), and AlexaFluor<sub>633</sub> (excitation 633 nm, emission 648–669 nm). The DAPI-stained nuclei and WGA-labeled apical membranes were used for orientation purposes but for the sake of clarity they have been omitted from Figure 1A.

## 2.6 | Immunohistochemistry of paraffin-embedded tissue

Mammary tissue was fixed in a mixture of 60% methanol, 30% chloroform, and 10% acetic acid overnight at 4°C, and sequentially dehydrated in ethanol immersed in 1,1,1, trichloroethane and embedded in paraffin or Paraplast Plus, as described.<sup>22</sup> Sections (7  $\mu$ m) were dewaxed with Histoclear (HS-200, National Diagnostics), rehydrated through a descending series of ethanol/water mixtures, and then immersed in 10 mM citrate buffer, pH 6.0 to retrieve antigen by heating in a pressure cooker for 1 min.<sup>23</sup> Endogenous peroxidase was

quenched by incubating the sections in 0.6% H<sub>2</sub>O<sub>2</sub>/100% methanol for 30 min and the sections then rehydrated in water for 5 min. After blocking with 10% normal goat serum for 1 h, sections were incubated with 1- to 100-fold dilutions of primary antibodies to either pStat3, pStat5, or Ki67 overnight at 4°C, followed by 1- to 50-fold dilutions of mouse biotinylated anti-rabbit IgG and avidin-HRP, according to the ABC VectorStain procedure (Vector Laboratories, Burlingame, CA). Sections were washed with PBS, and then stained with diaminobenzidine and counterstained with Harris's hematoxylin.

Cathepsin B was detected by immunofluorescence microscopy using paraffin-embedded tissue sections, which were dewaxed and heated to retrieve antigen, as above. Sections were incubated with 1- to 50-fold dilutions of rabbit anti-(human cathepsin B) (Thermo) and rat anti-(mouse lamp2) antibodies (Table S1) overnight at 4°C, washed with PBS and then incubated with 1- to 500-fold dilutions of goat anti-(rabbit IgG)-AlexaFluor<sub>488</sub> and goat anti-(rat-IgG)-AlexaFluor<sub>555</sub> antibodies for 1 h at room temperature. Sections were mounted in ProLong Gold™ Mountant with DAPI (Invitrogen) and examined with a Zeiss LSM780 confocal microscope (excitation BP 480/500 nm; emission 510–530 nm for cathepsin B and excitation BP 540/560 nm; emission 565–585 nm for Lamp2).

## 2.7 | Electron microscopy

Mammary tissue was fixed with a mixture of 2.5% (w/v) glutaraldehyde and 2% (w/v) OsO<sub>4</sub>, post-fixed with 2% (w/v) OsO<sub>4</sub><sup>24</sup> and embedded in Epon. Osmium-stained lipid was directly identified by Nomarski optics in thin sections with a Leica DMIRE2 microscope. Sections for electron microscopy were stained with uranyl acetate and lead citrate and examined with a Zeiss EM10CA electron microscope.

## 2.8 | Apoptosis assays

Cryostat sections (10  $\mu$ m) of unfixed frozen mammary gland from *Btn1a1*<sup>+/+</sup> and *Btn1a1*<sup>-/-</sup> mice at day 10 of lactation and *Btn1a1*<sup>+/+</sup> mice at day 2 of involution were analyzed by the TUNEL assay<sup>25</sup> to identify apoptotic cells. Sections were thawed and fixed with 4% (w/v) paraformaldehyde in PBS, pH 7.4 for 20 min at room temperature, washed for 30 min with PBS and permeabilized for 2 min with 0.1% (v/v) Triton-X-100/0.1% (w/v) sodium citrate on ice. Sections were washed a further two times with PBS and incubated with TUNEL reaction mixture (In situ

Cell Death Detection Kit, Fluorescein; Roche) for 1 h at 37°C in a humidity chamber in the dark. After two final PBS washes, sections were mounted in Vectashield® with DAPI and examined with a Leica SP5X confocal microscope using either a 40X oil (NA 1.25), or 63X oil (NA 1.4) objective and scanned sequentially for DAPI (excitation 405 nm, emission 413–435 nm) and fluorescein (excitation 488 nm, emission 499–559 nm). Fluorescein-positive and DAPI-stained nuclei were counted with the aid of ImagePro software (Media Cybernetics, Rockville, MD) and the number of apoptotic cells recorded as a percentile ratio.

In addition, 4% (w/v)-paraformaldehyde-fixed, frozen mammary tissue from *Btn1a1*<sup>+/+</sup> and *Btn1a1*<sup>-/-</sup> mice at day 10 of lactation was cut into 10 µm sections, thawed, permeabilized with Triton X-100 (0.2%, v/v) in PBS, incubated in a humidity chamber for 15 min and blocked with 2% (w/v) BSA/ 0.2% (v/v) Triton X-100 in PBS for 1 h. Sections were washed in PBS three times, incubated with rabbit anti-(mouse-cleaved caspase 3) (Table S1) at a 1- to 1,000-fold dilution, followed by a 1- to 1:500-fold dilution of goat anti-(rabbit IgG)-AlexaFluor<sub>568</sub> as secondary detecting agent and WGA-AlexaFluor<sub>633</sub> to label apical surfaces. Sections were mounted in Vectashield® with DAPI and cleaved caspase 3 positive cells identified with a Leica SP5X confocal microscope using either a 20X (NA 0.8) or 40X oil (NA 1.25) objective and sequential scans for DAPI (excitation 405 nm, emission 413–435 nm), AlexaFluor<sub>568</sub> (excitation 568 nm, emission 582–622 nm), and AlexaFluor<sub>633</sub> (excitation 633 nm, emission 644–670 nm).

## 2.9 | Isolation of RNA for qRT-PCR and RNAseq

For qRT-PCR, total RNA from day 5 lactating mammary glands was prepared from six each, *Btn1a1*<sup>+/+</sup> and *Btn1a1*<sup>-/-</sup> mice using TRIzol reagent (Invitrogen) and the isolated RNA purified using a Qiagen RNeasy cleanup kit (Valencia, CA). For RNAseq, total RNA was isolated from the mammary glands of five *Btn1a1*<sup>+/+</sup> and seven *Btn1a1*<sup>-/-</sup> mice (days 9–11 of lactation) using Tri Reagent® and an associated kit from Zymo Research Corp (Irvine, CA). In all cases, samples were stored immediately after isolation in RNase-free water at -80°C.

### 2.9.1 | Quantitative real time polymerase chain reaction (qRT-PCR)

cDNAs complimentary to selected genes were synthesized using a SuperScript™ III One-Step RT-PCR kit from

Invitrogen and the primer pairs listed in Table S3. For qRT-PCR analysis, 4 µl of diluted cDNA was combined with 15 µl of a mixture comprising 10 µl 1x SYBR Green master mix (IQ™ SYBR® Green Supermix), 0.8 µl each of 10 µM forward and reverse primers, and 4.4 µl DNase/RNase-free water in a 96-well iCycler iQ Real-time PCR Detection system (Bio-Rad). Each sample was amplified in triplicate and a 4-point relative standard curve (4-fold dilution) and a non-template control included. Amplification reactions were: - 2 min at 50°C and 10 min at 95°C, followed by 40 cycles of 15 s at 95°C, and 1 min at 60°C. The presence of a single PCR product was verified by the dissociation protocol using incremental temperatures to 95°C for 15 sec plus 65°C for 15 s. The geometric mean of Slc44a3 and SPG21 genes, the most stable genes from the RNAseq were used for normalization of qRT-PCR data. Data were analyzed with 7900 HT Sequence Detection Systems Software (version 2.2.3, Applied Biosystems). RNA from 6 *Btn1a1*<sup>+/+</sup> and *Btn1a1*<sup>-/-</sup> mice were analyzed in duplicate.

### 2.9.2 | Gene expression analysis of *Btn1a1*<sup>+/+</sup> and *Btn1a1*<sup>-/-</sup> mice by RNAseq

Total mammary RNA from five *Btn1a1*<sup>+/+</sup> and seven *Btn1a1*<sup>-/-</sup> mice were analyzed for integrity by Agilent RNA nano assay on a bioanalyzer. All samples had acceptable RNA integrity numbers (RIN) between 8.2 and 9.6. Total RNA (2 µg/sample) was fractionated using an Illumina TruSeq mRNA library preparation kit to isolate mRNA by capture on oligo-dT coated magnetic beads. The mRNA was then fragmented and converted to double-stranded cDNA by random-primed cDNA synthesis. Standard Illumina libraries were prepared from the double-stranded cDNAs with end-repair, adapter ligation, and PCR amplification to generate sequencing ready libraries. The final purified products were then quantitated by qPCR before cluster generation and sequencing on an Illumina HiSeq 4000 sequencer using an Illumina HiSeq SBS kit and paired-end sequencing. Details of all Illumina protocols can be found on their website (<https://www.illumina.com/>).

RNA sequencing sample reads were processed using the CCBP Pipeliner utility (<https://github.com/CCBR/Pipeliner>). The samples had 95 to 167 million pass filter reads with more than 92% of bases above the quality score of Q30. Briefly, reads of the samples were trimmed for adapters and low-quality bases using Cutadapt (v1.18)<sup>26</sup> before alignment with the reference genome (Mouse - mm10) and the annotated transcripts using STAR v2.4.2a in 2-pass mode.<sup>27</sup> The average mapping rate of all samples was above 97%. Unique alignment was above 80%. There were 2.09%–2.63% unmapped

reads. The mapping statistics were calculated using Picard software (<http://broadinstitute.github.io/picard/>). The samples had 0.09% ribosomal bases. Percent coding bases were between 65 and 70%. Percent UTR bases were 26%–29%, and mRNA bases were between 94% and 96% for all the samples. Library complexity was measured in terms of unique fragments in the mapped reads using Picard's MarkDuplicate utility. The samples had 9%–16% non-duplicate reads. The RNAseq data have been deposited in NCBI's Gene Expression Omnibus (GEO) repository and are available through GEO series accession number GSE-182075 (<https://www.ncbi.nlm.nih.gov/geo/query/acc.cgi?acc=GSE182075>).

## 2.10 | Proteomic analysis of mammary tissue from *Btn1a1*<sup>+/+</sup> and *Btn1a1*<sup>-/-</sup> mice

Proteins were reduced, alkylated, and digested with trypsin overnight at 37°C using S traps (ProtiFi), following the manufacturer's protocol. The peptides were acidified and desalted on a C18 SepPak cartridge (Waters) and dried by vacuum concentration (Labconco). Dried peptides were fractionated with high pH reversed-phase spin columns (Thermo). The peptides from each fraction were lyophilized prior to mass spectrometry analysis. In order to avoid potential batch effects,<sup>28</sup> *Btn1a1*<sup>+/+</sup> and *Btn1a1*<sup>-/-</sup> samples were analyzed in random order. Each fraction of each sample was separated on a 75  $\mu\text{m}$   $\times$  15 cm, 2  $\mu\text{m}$  Acclaim PepMap reverse phase column (Thermo) using an UltiMate 3000 RSLCnano HPLC (Thermo) at a flow rate of 300 nl/min followed by online analysis by tandem mass spectrometry using a Thermo Orbitrap Fusion mass spectrometer. Peptides were eluted into the mass spectrometer using a 120 min gradient. Parent full-scan mass spectra were collected in the Orbitrap mass analyzer set to acquire data at 120,000 FWHM resolution; ions were then isolated in the quadrupole mass filter, fragmented within the HCD cell (HCD normalized energy 32%, stepped  $\pm 3\%$ ), and the product ions analyzed in the ion trap. The mass spectrometry data were analyzed in Proteome Discoverer 2.3 (Thermo). Proteins were searched against murine proteins from the UniProt database using SequestHT (database downloaded 02/2019, release 2019\_01). The search was limited to tryptic peptides, with maximally two missed cleavages allowed. Cysteine carbamidomethylation was set as a fixed modification, and methionine oxidation set as a variable modification. The precursor mass tolerance was 10 ppm, and the fragment mass tolerance was 0.6 Da. The Percolator node was used to score and rank peptide matches using a 1% false discovery rate. The Minora and Precursor Ion Quantifier nodes in Proteome Discoverer were used for label-free detection. Normalization was done using total peptide amount and the peptide ratio was

calculated using pairwise ratios, in which the peptide group ratios are calculated as the geometric median of all combinations of ratios from all the replicates and the protein ratio is subsequently calculated as the geometric median of the peptide group ratios. The mass spectrometry proteomics data have been deposited to the ProteomeXchange Consortium via the PRIDE<sup>29</sup> partner repository with the dataset identifier PXD021249 and 10.6019/PXD021249.

## 2.11 | Bioinformatics of RNAseq and proteomic data

Expression levels were quantified using RSEM (v1.3.0)<sup>30</sup> with GENCODE annotation version M18 (GRCm38; Ensembl 93). Raw read counts (expected counts from RSEM) were imported into the NIH Integrated Data Analysis Platform for downstream analysis (<https://nidap.nih.gov/>). Only those genes with >1 count-per-million (CPM) in at least three samples per group were analyzed. Counts were normalized to library size as  $\log_2\text{CPM}$  and the voom algorithm<sup>31</sup> from the Limma R package (v3.40.6)<sup>32</sup> as used for quantile normalization. Differentially expressed gene (DEG) analysis was performed using Limma and pre-ranked gene set enrichment analysis (GSEA)<sup>33</sup> as performed using the molecular signatures database v6.2.<sup>34</sup> Genes or gene sets with an adj. *p* value of  $\leq 0.05$  was considered statistically significant. The Ingenuity Pathway Analysis (IPA) software from Qiagen Inc. was used to further explore and visualize those significant pathways detected (<https://www.qiagenbioinformatics.com/products/ingenuitypathway-analysis>). The Integrated Genomics Viewer (IGV) was used to visualize read pile-ups (BAM files) along the gene annotation and to produce the Sashimi plots in Figure A1.<sup>35</sup>

For the proteomic data, differentially expressed pathways were identified using MetaCore software (Clarivate Analytics, Philadelphia, PA) Gene Ontology (GO) enrichment analysis (Version 20.4 Build 70300). Significant data ( $\pm 2$ -fold, null/wild type;  $p \leq 0.05$ ) were analyzed for significantly enriched gene pathways and networks within the Ontology Categories, Pathway Maps, Process Networks and Metabolic Networks (Endogenous), and the GO Categories: Processes, Localizations, and Molecular Functions.

### 2.11.1 | Assays

Lipid peroxidation was measured indirectly by estimating the amount of malondialdehyde (MDA) in milk lipid and PNS tissue samples with a kit from Sigma-Aldrich (St. Louis, MO). Samples of milk lipid (10  $\mu\text{l}$ ) were briefly melted at 40°C in 300  $\mu\text{l}$  proprietary MDA lysis buffer containing 3  $\mu\text{l}$  of butylated hydroxytoluene (BHT) and centrifuged at

13,000 g<sub>av</sub> for 10 min at 4°C. PNS samples (20 µl, approx. 300 µg) were added to the same lysis buffer/BHT mixture on ice and centrifuged as above. Aliquots (200 µl) of either the lipid or PNS fractions were then treated with 600 µl thio-barbituric acid reagent in 30% (v/v) acetic acid and heated to 95°C for 60 min. Absorbance of the pink/orange-colored MDA-TBA adduct was spectrophotometrically measured at 532 nm and compared against a set of MDA standards (0–20 nmol). Attempts to analyze skim milk samples by similar procedures were compromised by interference from reactive substances absorbing at lower wavelengths.

Oxidized residues in proteins (3-nitrotyrosine and carbonyl groups) were assayed by immunoblot using kits from Cell BioLabs Inc (San Diego, CA). Nitrotyrosine was detected on blots of PNS fractions with a specific rabbit antibody (Table S1) and intensity of the chemiluminescent signals compared with that of a nitrotyrosine-BSA control. Carbonyl groups in blotted PNS samples were measured indirectly by reaction with dinitrophenylhydrazine, which forms dinitrophenylhydrazone derivatives that can be detected with a specific rabbit antibody to dinitrophenol. Carbonyl-BSA, prepared by incubation of BSA (5 mg/ml) with 25 mM ascorbic acid and 100 µM FeCl<sub>3</sub> overnight at 37°C served as a reference.

Xdh (oxidase activity) was assayed aerobically in 100 mM sodium phosphate buffer, pH 7.2, containing 10% (v/v) dimethyl sulfoxide and 150 µM xanthine at 37°C. The conversion of xanthine into uric acid was followed at 293 nm using a PerkinElmer Life Sciences Lambda 25 spectrophotometer. Enzyme activity (IU) was calculated using a molar extinction coefficient for uric acid under the assay conditions of  $12.5 \times 10^3 \text{ M}^{-1} \text{ cm}^{-1}$ .

Protein was assayed either by the Bradford method<sup>36</sup> or with the bicinchoninic acid reagent<sup>37</sup> using BSA as a standard.

## 2.12 | Statistical analysis

The RNAseq and proteomic data were analyzed for statistical significance (null/wild type,  $\pm 2$ -fold, adj. *p* values  $\leq 0.05$ ) as indicated in Sections 2.9.2–2.11. All other data were analyzed for significance with the F test (ANOVA) as indicated in the figure legends.

## 3 | RESULTS

### 3.1 | Xdh protein accumulates in the cytoplasm of *Btn1a1*<sup>-/-</sup> mice

The genesis of this research lies in the chance discovery that Xdh, a major binding partner of Btn1a1,

is highly enriched in the cytoplasm of milk-secreting mammary cells in *Btn1a1* null mice. Using immunocytochemistry and an anti-peptide antibody to mouse Xdh, a strong positive signal was observed throughout the cytoplasm of unfixed sections of mammary tissue in *Btn1a1*<sup>-/-</sup> mice, compared with wild type controls (Figure 1A,a,c). Furthermore, there was a distinct difference in Xdh distribution between the two genotypes; Xdh was enriched in the apical regions of *Btn1a1*<sup>+/+</sup> cells, compared with a more intense and global fluorescent signal in null cells. This implied that Btn1a1, which is targeted to the apical plasma membrane,<sup>1,38</sup> modulates the distribution and concentration levels of Xdh in wild type cells. To test this possibility, the soluble and membrane-bound fractions of Xdh in mammary cells were identified by removing unbound Xdh from parallel sections, which were treated with digitonin to permeabilize membranes and wash out soluble proteins. Following digitonin treatment, a fraction of Xdh remained associated with the apical membrane in *Btn1a1*<sup>+/+</sup> cells (Figure 1A,a,b) but strikingly most Xdh was washed out of the knockout tissue (Figure 1A,c,d). These results imply that a fraction of Xdh is bound to the apical pole in wild type cells, and that loss of Btn1a1 as an anchor results in redistribution of most Xdh molecules to the cytoplasm. There also appeared to be an absolute increase in the quantity of Xdh in *Btn1a1*<sup>-/-</sup> cells compared with wild type.

To confirm that Xdh is expressed at higher levels in *Btn1a1*<sup>-/-</sup> cells, we assessed the relative amounts of Xdh protein in mammary cell fractions by western immunoblot (Figure 1B,C). Qualitative analysis showed stepwise increases in Xdh, especially in post-microsomal supernatant fractions, as the amount of Btn1a1 decreased between *Btn1a1*<sup>+/+</sup>, *Btn1a1*<sup>+/-</sup>, and *Btn1a1*<sup>-/-</sup> mice (Figure 1B). By quantitative immunoblot, there was a statistically significant 6.7-fold increase (*p* < 0.05) in the total amount of Xdh at peak lactation in *Btn1a1*<sup>-/-</sup> mice compared with *Btn1a1*<sup>+/+</sup> animals. Following weaning, Xdh in wild type animals were sustained for at least the first 2 days of involution, (Figure 1C, Table S4). An analysis of six genotypes, including animals with disruptions in both *Btn1a1* and *Xdh* genes, revealed an inverse relationship between the amount of Btn1a1 and Xdh using enzyme activity as a measure of Xdh (Figure 1D,E). Xdh amounts increased to a maximum of 5.65-fold in *Btn1a1*<sup>-/-</sup> mice relative to wild type (Figure 1D), with other genotypes comprising disruptions in either one or both genes falling in between (Figure 1D,E). Thus, the total amount of Xdh in cells is inversely related to the expression of Btn1a1.



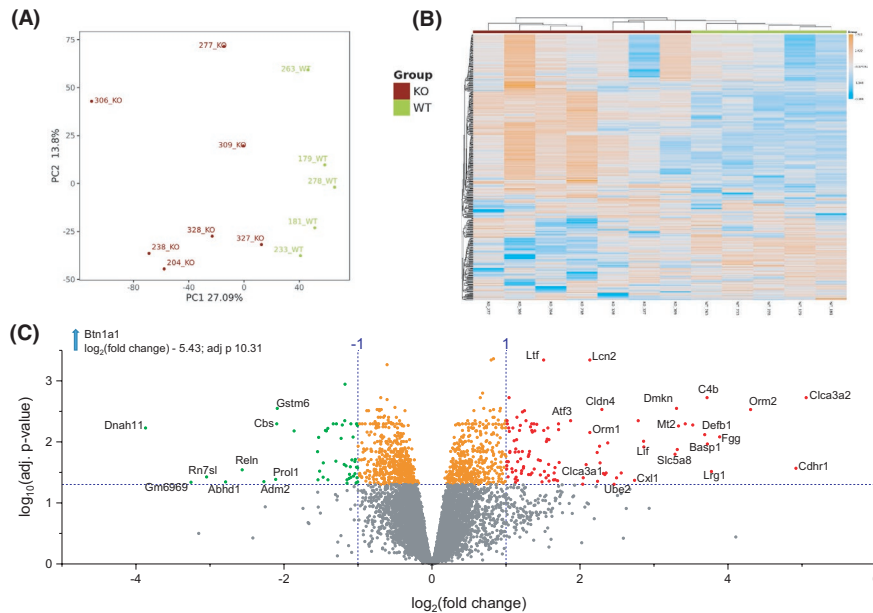


**FIGURE 2** Comparative RNAseq analysis of *Btn1a1*<sup>+/+</sup> and *Btn1a1*<sup>-/-</sup> mice. (A) Principal component analysis of normalized RNAseq metadata from five *Btn1a1*<sup>+/+</sup> (green) and seven *Btn1a1*<sup>-/-</sup> (purple) mice showing a significant and consistent divergence in gene expression levels between the two genotypes. (B) Heat map of the mRNAs from the five *Btn1a1*<sup>+/+</sup> (green) and seven *Btn1a1*<sup>-/-</sup> (purple) mice summarized in (A). Downregulated and upregulated genes are shown on a sliding blue to orange scale. (C) Volcano plot of fold changes of the amounts of specific mRNAs in the mice summarized in (A). mRNAs upregulated or downregulated more than twofold (null/wild type) with adj. *p* values ≤ 0.05 are shown to the right and left of the figure as red or green dots, respectively above the dotted line. To expand the y axis, the point for *Btn1a1* mRNA, which is downregulated 43.2-fold is omitted and the specific data are shown in the top left hand corner

A Gene Set Enrichment Analysis<sup>33</sup> of the RNAseq data for four gene set collections (GO, HALLMARK, KEGG, and REACTOME) is filed in Excel Spreadsheets 4–7. Hierarchical clustering of the 721 most significant GO gene set pathways (adj. *p* values < 0.05) showed enrichment (null/wild type) in pathways associated with upregulation of the cell cycle, cytoskeleton, inflammation, and apoptosis and downregulation of pathways associated with lipid and amino acid metabolism. Similar trends were evident in the other gene set collections analyzed (examples, Figure S1). Four of the top five canonical pathways identified by Ingenuity Pathway Analysis were associated with cell cycle control (example, Figure S2) and some of the most significant molecular and cellular functions comprised cell death and survival, the cell cycle, DNA replication, recombination, and repair (Excel Spreadsheet 8).

Significant changes in protein levels between the two genotypes (null/wild type ≥ ±2-fold; adj. *p* values ≤ 0.05) accounted for 18.2% of the total identified (611 up and 139 down, including 519 that were only detected in either *Btn1a1*<sup>+/+</sup> or *Btn1a1*<sup>-/-</sup> mice, encircled points, volcano plot, Figure 3A; Excel Spreadsheets 1,2). Only 10 mRNA/protein pairs were significantly upregulated using the same criteria for both mRNA and protein (null/wild type ≥

±2-fold; adj. *p* values ≤ 0.05, Excel Spreadsheet 3) and only *Btn1a1* mRNA/protein together was significantly downregulated. The abundance of degraded *Btn1a1* protein in knockout animals compared to wild type was estimated to be 5-fold decreased by pair-wise determination and 22-fold decreased by simple arithmetic ratio (Discussion and Appendix).

Despite the few significant coordinate changes in RNA and protein, MetaCore enrichment analysis of changes in protein alone or combined protein and RNA (null/wild type ≥ ±2-fold; adj. *p* values ≤ 0.05) were broadly in line with the above RNA analysis. Pathway, Process Networks, Metabolic Networks (Endogenous), and GO analyses of the 750 significantly changed proteins were consistent with inflammation and Il-6 signaling, autophagy, the cell cycle, apoptosis, optimal maintenance of cell architecture, membrane-bounded organelles, lipid metabolism, and transport functions (Figure 3B, C, 3SA, Excel Spreadsheets 9–14). Simultaneous analysis of all the RNA and protein data revealed enrichment in the genes and proteins associated with inflammation, the acute phase response and apoptosis (Figure 3D–G, S3B, Excel Spreadsheets 15–17).

Predicted associations with cell injury, inflammation, and death are in line with the physical damage to

**TABLE 1** Fold change in expression of the most upregulated or downregulated genes in the lactating mammary glands of *Btn1a1*<sup>-/-</sup> compared with *Btn1a1*<sup>+/+</sup> mice by RNAseq analysis

Gene	Description	Null/wild type ratio	adj <i>p</i> value <sup>†</sup>
Upregulated genes, highest to lowest (fold change ≥ 5.0)			
Clca3a2	Chloride channel accessory 3a2	33.26	0.002
Cdhr1	Cadherin-related family member 1	30.24	0.027
Orm2	a-1-acid glycoprotein 2, Orosomuroid 2	19.77	0.003
Fgg	Fibrinogen gamma chain	14.80	0.008
Lrg1	Leucine-rich a2 glycoprotein 1	13.71	0.031
Basp1	Brain-abundant membrane-attached signal protein 1	13.20	0.011
C4b	Complement C4b (Chido blood group)	13.15	0.002
Defb1	Defensin β1	12.87	0.008
Spp1	Secreted phosphoprotein 1	11.51	0.005
Mt2	Metallothionein 2	10.72	0.005
Dmkn	Dermokine	10.07	0.005
S100a14	S100 calcium binding protein A14 protein	9.95	0.013
Slc5a8	Solute carrier family 5, member 8	9.75	0.016
Lif	Lif interleukin 6 family cytokine	7.27	0.012
Ankrd1	Ankyrin repeat domain 1	7.26	0.010
Cldn4	Claudin4 /mCPE receptor	6.90	0.004
Cxcl1	C-X-C motif chemokine ligand 1 (KC)	6.67	0.043
Wfdc17	WAP four-disulfide core domain 17	5.89	0.032
Fign1	Fidgetin-like 1	5.63	0.039
Ube2c	Ubiquitin conjugating enzyme E2c	5.50	0.049
Orm1	Orosomuroid 1	5.19	0.010
Slc41a2	Solute carrier family 41, member 2	5.11	0.032
Clca3a1	Chloride channel accessory 3a2	5.04	0.034
Downregulated genes, most to least (fold change ≥ 4.0)			
Btn1a1	Butyrophilin family member 1a1	-43.21	4.95E-11
Dnah11	Dynein axonemal heavy chain 11	-14.63	0.006
Gm6969	Predicted pseudo gene 6969	-9.55	0.046
Rn7s1	7S RNA1	-8.26	0.038
Abhd1	Abhydrolase domain containing 1	-6.91	0.045
Reln	Reelin	-5.92	0.029
Adm2	Adrenomedullin 2	-4.83	0.045
Prol1	Opiorphin prepropeptide	-4.32	0.041
Cbs	Cystathionine β-synthase	-4.28	0.005
Gstm6	Glutathione S-transferase Mu 6	-4.26	0.003

Upregulated Riken genes, 2610528A11Rik and E330013P04Rik are omitted from list.

<sup>†</sup>Only significantly changed transcripts are listed (adj. *p* value ≤ 0.05). Of note, *Saa1*, 2 and 3 showed large changes in RNA null/wild type ratios, which were not significant (See Excel Spreadsheet 1 and Table 2 for significant changes in protein).

mammary-cell structures observed in *Btn1a1*<sup>-/-</sup> mice caused by the accumulation of large LDs in the cytoplasm (Figure S4).<sup>13</sup> On the other hand, upregulation of pathways required for DNA repair, synthesis, and mitosis suggests that the gland is simultaneously undergoing cell replacement and epithelial renewal.

### 3.3 | Cell death is significant in the lactating mammary glands of *Btn1a1*<sup>-/-</sup> mice

To confirm cell death within the mammary epithelia of null mice at peak lactation, we used the TUNEL assay to

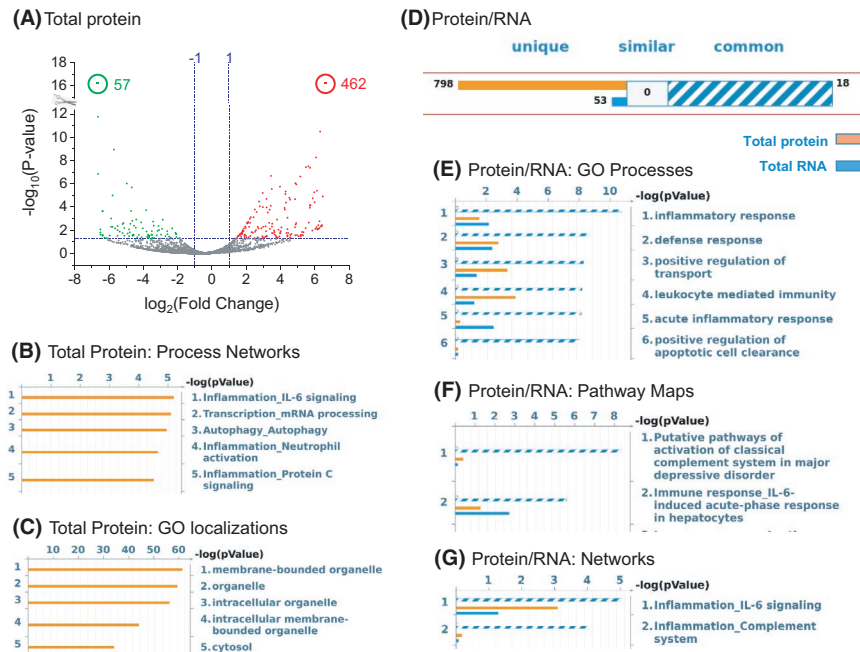


**FIGURE 3** Comparative proteomic and combined RNAseq and proteomic analysis of post-nuclear supernatants from *Btn1a1*<sup>+/+</sup> and *Btn1a1*<sup>-/-</sup> mice. (A) Volcano plot of fold changes of proteins upregulated or downregulated more than twofold (null/wild type) with adj. *p* values  $\leq 0.05$ , shown to the right and left of the figure as red or green dots, respectively above the dotted line. A total of 519 proteins were either absent (57) or only present (462) in *Btn1a1*<sup>-/-</sup> mice and therefore have infinite  $\pm$ fold-changes and adj. *p* values (encircled points). See complete lists in Excel Spreadsheet 2. (B, C) MetaCore enrichment analysis of the significantly changed proteins in Volcano plot A, for B. Process Networks and C. GO Localizations. For comprehensive details of Metacore protein analysis see Excel Spreadsheets 9–14. (D–G) Enrichment analysis of the intersections between total mRNA and protein data sets mapped onto MetaCore's functional ontologies [mRNAs and proteins upregulated or downregulated more than twofold (null/wild type), adj. *p* values  $\leq 0.05$ ]. (D) Summary of possible targets for common (blue striped box), similar (empty box), and unique [orange box, protein, blue box mRNA] MetaCore gene sets. (E) GO Processes, (F) Pathway Maps, (G) Networks. For comprehensive details see Excel Spreadsheets 15–17

estimate the abundance of nuclei containing DNA with double-strand breaks,<sup>25</sup> and immunofluorescence to detect the expression of active caspase 3.<sup>39</sup> Mammary epithelial cells were compared in *Btn1a1*<sup>+/+</sup> and *Btn1a1*<sup>-/-</sup> mice at day 10 of lactation with cells in wild type mice at 2 days after weaning. Approximately 10% of the cells in *Btn1a1*<sup>-/-</sup> mice at peak lactation were positive in the TUNEL assay, a value that was indistinguishable from the level in involuting wild type cells (Figure 4A,B, Table S4). In addition, a number of cells were positive for active caspase 3 in null mice, whereas virtually all wild type cells were negative at the same stage of lactation (Figure 4C). This increase in active caspase 3 was not due to increased protein synthesis as both caspase 3 mRNA and protein levels were significantly downregulated (Table 2). Also, despite an insignificant change in mRNA levels, there was a significant increase in caspase 8 protein (Excel Spreadsheets 1,2, Table 2).

Cell death during involution in mammary cells is initiated by Lif-induced phosphorylation of the transcription factor, signal transducer and activator of transcription

(Stat) 3, and translocation of phosphorylated Stat3 (pStat3) into the nucleus.<sup>40,41</sup> A comparison of the distribution of pStat3 by immunohistochemistry at day 10 of lactation showed accumulation of pStat3 in the nuclei of *Btn1a1*<sup>-/-</sup> cells, lower amounts in the epithelia of heterozygotes and none in wild type cells (Figure 5A). Wild-type tissue from day 1 of involution served as a positive control and displayed the most intense staining. Immunoblots confirmed phosphorylation of Stat3 in *Btn1a1*<sup>-/-</sup> tissue at peak lactation, which was statistically similar to the amount at early stages of involution in wild type mice (Figure 5B,C). Against a constant background expression of Stat3, the ratio of pStat3 to Stat3 rose from 0.007 in wild type tissue to 0.44–0.48 in both the *Btn1a1*<sup>-/-</sup> mice at peak lactation and *Btn1a1*<sup>+/+</sup> mice in the first 2 days of involution (Figure 5C; Table S4). In comparison, pStat5 which is essential for lactogenesis and the maintenance of milk secretion<sup>42</sup> was detected in the nuclei of epithelia from all three genotypes at day 10 of lactation, and in wild type cells at day 1 of involution (Figure 5D). As expected, the ratio of pStat5 to Stat5 remained elevated in differentiated

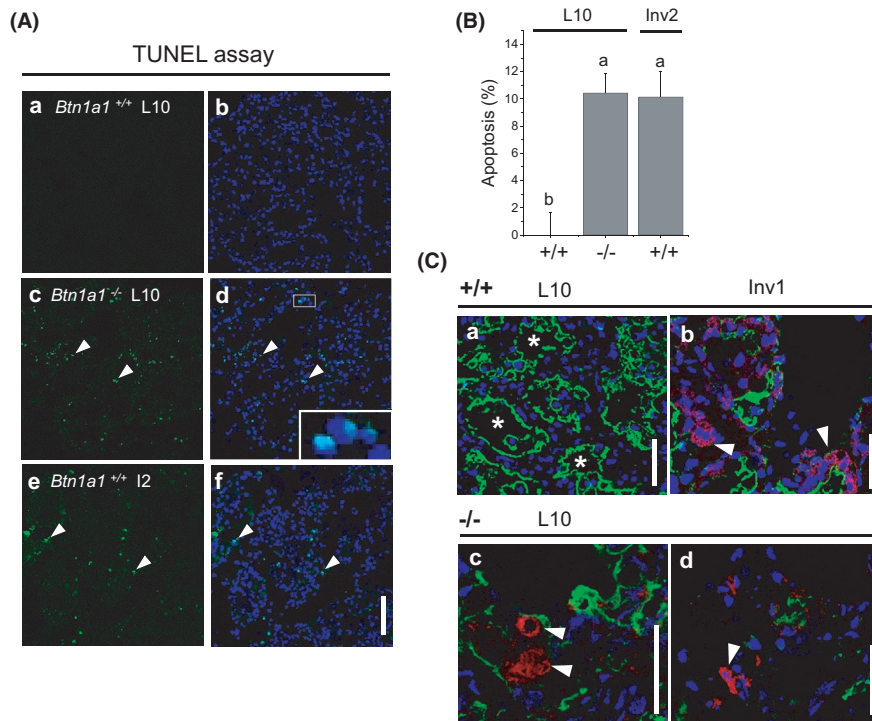


**FIGURE 4** Loss of *Btn1a1* leads to increased cell death in the lactating mammary gland. (A) Flash-frozen, thawed and 4% paraformaldehyde-fixed tissue sections from *Btn1a1*<sup>+/+</sup> and *Btn1a1*<sup>-/-</sup> mice were analyzed by the TUNEL assay to identify apoptotic cells. (a, b) *Btn1a1*<sup>+/+</sup> mice at day 10 of lactation, (c, d) *Btn1a1*<sup>-/-</sup> mice at day 10 of lactation, (e, f) *Btn1a1*<sup>+/+</sup> mice at day 2 of involution (Inv 2). (a, c, e) TUNEL assay, (b, d, f) merged images showing DAPI-stained nuclei (blue). TUNEL-positive nuclei are shown in green (arrowheads) and boxed inset in (d). Bar 50  $\mu$ m. (B) Number of apoptotic cells (%) in *Btn1a1*<sup>+/+</sup> and *Btn1a1*<sup>-/-</sup> mice at day 10 of lactation, and *Btn1a1*<sup>+/+</sup> mice at day 2 of involution. (n = 3; 1,000 cells/mouse). Columns with different letters are statistically different from each other. Means  $\pm$  SEM,  $p < 0.05$ , F-test (ANOVA). (C) Loss of *Btn1a1* leads to the appearance of cleaved caspase 3 in the secretory epithelium. (a–d) Fixed, frozen mammary gland sections (10  $\mu$ m) were thawed and stained for cleaved-caspase-3 as described in Materials and Methods. Sections were counter-stained with WGA to identify the apical plasma membrane. (a) *Btn1a1*<sup>+/+</sup> lactation day 10, (b) *Btn1a1*<sup>+/+</sup> involution, day 1 (Inv 1), (c, d) two examples, *Btn1a1*<sup>-/-</sup>, lactation day 10. Cleaved caspase-3 (red, white arrowheads), DAPI-stained nuclei (blue) and WGA (green). Representative examples from three mice/genotype. Asterisks, aveolar lumenae. Bars, 50  $\mu$ m

cells regardless of genotype at peak lactation but markedly declined during early involution (Figure 5E,F, Table S4).

Stat3 signaling precipitates cell death during mammary involution through the upregulation of cathepsins B and L, followed by leakage of these and other degradative enzymes from lysosomes into the cytoplasm.<sup>43</sup> Therefore, we compared the distribution of cathepsin B, with lamp2 as a marker of lysosomal membranes (Figure 6). There was a modest increase in the number of cathepsin-B positive lysosomes in null, compared with wild type and heterozygous mice, albeit at lower levels than in wild type involuting animals (arrowheads, puncta, Figure 6A,c,d). By immunoblot, amounts of cathepsin B were increased but highly variable among animals (Figure 6B; Table S4). Strikingly, lamp2 was detected in extra-lysosomal structures, especially in apical regions, in both lactating null and wild type involuting mice, compared with wild type or heterozygous controls (Figure 6A,c,d), presumably because endogenous recycling of lamp2 through the

endosomal system from the apical surface to lysosomes was disrupted. These results are consistent with a role for lysosomal enzymes in cell death at peak lactation in *Btn1a1*<sup>-/-</sup> mice through a modest pStat3-mediated increase in cathepsins, which is accompanied by extensive redistribution of lysosomal content and membranes (but see Discussion for caveats).

The massive accumulation of Xdh in *Btn1a1*<sup>-/-</sup> cells raised the interesting possibility that Xdh-generated reactive oxygen species initiate cell death through oxidative damage to both lipids and proteins. PNS fractions and milk lipid samples from *Btn1a1*<sup>+/+</sup>, *Btn1a1*<sup>+/-</sup>, and *Btn1a1*<sup>-/-</sup> mice were assayed using the thiobarbituric acid reagent (Figure S5A) for the presence of malondialdehyde (MDA), which is an end product of the peroxidation of polyunsaturated fatty acids.<sup>44</sup> There was a modest but statistically insignificant increase in MDA levels in *Btn1a1*<sup>+/-</sup> and *Btn1a1*<sup>-/-</sup> tissue samples, compared with wild type and only one of four *Btn1a1*<sup>-/-</sup> milk lipid samples

**TABLE 2** Fold change in expression of selected genes and encoded proteins in the lactating mammary glands of *Btn1a1*<sup>-/-</sup> compared with *Btn1a1*<sup>+/+</sup> mice

Gene symbol	Gene description	mRNA null/wild type <sup>†</sup>	adj. p value	Protein null/wild type <sup>†</sup>	adj. p value
Involution Phase 1: 0-48h					
Atp2b2	ATPase PM Ca <sup>2+</sup> transporting 2 (Pmc2a)	-1.48	0.04	0.60	0.97
Atp2c2	ATPase sec. path. Ca <sup>2+</sup> transporting 2	-1.40	0.03	0.39	0.68
Clu	sulfated glycoprotein-2, clusterin	<b>1.93</b>	<b>0.01</b>	2.19	0.14
Ctsb	cathepsin b	1.17	0.29	0.91	0.97
Ctsd	cathepsin d	1.08	0.36	1.60	0.38
Lbp	lipopolysaccharide binding protein	<b>1.60</b>	<b>0.01</b>	1.42	0.78
Lif	Lif interleukin 6 family cytokine	<b>7.27</b>	<b>0.01</b>	ND <sup>‡</sup>	N/A <sup>‡</sup>
Lrg1	leucine-rich a2 glycoprotein 1	<b>13.70</b>	<b>0.03</b>	ND	N/A
Orm1	orosomucoid1	<b>5.19</b>	<b>0.01</b>	<b>&gt;100<sup>§</sup></b>	<b>5.80E-17</b>
Orm2	orosomucoid 2, a-1-acid glycoprotein 2	<b>19.77</b>	<b>0.003</b>	<b>4.50</b>	<b>0.005</b>
Saa1	serum amyloid 1	<b>177.9</b>	<b>0.08</b>	<b>7.85</b>	<b>0.0001</b>
Saa2	serum amyloid 2	264.9	0.18	<b>&gt;100</b>	<b>5.80E-17</b>
Serpina3g	serpin family a member 3g (Spi2a)	1.62	0.38	ND	N/A
Slc9a3r1	Slc9a3 regulator 1 (Nherf1)	-1.16	0.12	0.65	0.88
Slpi	secretory leukocyte protease inhibitor	<b>3.20</b>	<b>0.08</b>	ND	N/A
Socs3	suppressor of cytokine signaling 3	2.23	0.14	ND	N/A
Stat3	signal transducer activator of transcript. 3	1.42	0.04	0.72	0.99
Timp1	tissue inhibitor of metalloproteinase1	<b>1.90</b>	<b>0.003</b>	ND	N/A
Tnf	tumor necrosis factor (Tnfa)	ND	N/A	ND	N/A
Involution Phase 2: 48-96h					
Arg1	arginase 1	<b>4.81</b>	<b>0.01</b>	ND	N/A
Chil3	chitinase-like protein 3 (Ym1)	ND	N/A	ND	N/A
Clca1	Cl <sup>-</sup> channel Ca <sup>2+</sup> -activated 1	ND	N/A	ND	N/A
Clca2	Cl <sup>-</sup> channel Ca <sup>2+</sup> -activated 2	<b>2.87</b>	<b>0.03</b>	ND	N/A
Klkb1	kallikrien b1	ND	N/A	ND	N/A
Mmp2	gelatinase A, matrix metalloproteinase 2	1.11	0.64	ND	N/A
Mmp3	stromelysin-1, matrix metalloproteinase 3	1.45	0.27	ND	N/A
Mmp9	gelatinase B, matrix metalloproteinase 9	ND	N/A	ND	N/A
Mmp12	elastase, matrix metalloproteinase 12	<b>1.61</b>	<b>0.02</b>	ND	N/A
Mmp14	matrix metalloproteinase 14	1.23	0.25	ND	N/A
Osm	oncostatin M	ND	N/A	ND	N/A
Osmr	oncostatin M receptor	1.38	0.14	ND	N/A
Plat	plaminogen activator, tissue type	-1.05	0.86	ND	N/A

(Continues)

TABLE 2 (Continued)

Gene symbol	Gene description	mRNA null/wild type <sup>†</sup>	adj. p value	Protein null/wild type <sup>†</sup>	adj. p value
Plau	urokinase-type plasminogen activator	1.36	0.06	ND	N/A
Plaur	plasminogen activator, urokinase receptor	1.94	0.19	ND	N/A
Stat6	signal transducer activator of transcript. 6	-1.15	0.07	<b>0.12</b>	<b>0</b>
Unfolded protein response					
Atf4	Activating transcription factor 4	-1.01	0.91	ND	N/A
Atf6	Activating transcription factor 6	1.11	0.55	ND	N/A
Ddit3	DNA damage inducible transcript 3 (Chop)	-1.02	0.93	ND	N/A
Eif2 $\alpha$	Eukary. transl. init.. factor 2 $\alpha$	1.05	0.57	0.77	1.00
Eif2ak3	Eukary. transl. init. factor 2 $\alpha$ kinase 3 (Perk) 1.09	0.64	0.68	1.00	
Ern1	ER signaling to nucleus 1 (Ire1)	-1.11	0.29	ND	N/A
Hspa5	Heat shock family protein a5 (Grp78)	1.31	0.21	1.54	0.49
Xbp1	X-box binding protein 1	1.01	0.96	ND	N/A
Autophagy					
Atg4b	autophagy-related 4b cysteine peptidase	1.02	0.82	<b>13.46</b>	<b>0.05</b>
Atg7	autophagy-related 7	1.0	0.97	<b>44.8</b>	<b>3.71E-08</b>
Atg16l1	autophagy-related 16-like 1	-1.06	<b>0.58</b>	<b>&gt;100</b>	<b>5.80E-17</b>
Becn1	beclin1	1.03	0.68	ND N/A	
Gabarapl2	GABA type A receptor assoc. protein-like 2	-1.10	<b>0.26</b>	<b>&gt;100</b>	<b>5.80E-17</b>
Map1lc3a	MT-assoc. protein 1 light chain 3 $\alpha$ (LC3 $\alpha$ )	1.27	0.07	ND	N/A
Map1lc3b	MT-assoc. protein 1 light chain 3 $\beta$ (LC3 $\beta$ )	1.04	0.70	<b>&gt;100</b>	<b>5.80E-17</b>
Tlr2	Toll-like receptor 2	1.07	0.72	<b>12.33</b>	<b>0.01</b>
Tlr3	Toll-like receptor 3	1.16	0.12	<b>&gt;100</b>	<b>5.80E-17</b>
Efferocytosis					
Aph1 $\alpha$	aph-1 homolog a, $\gamma$ -secretase subunit $\alpha$	1.08	0.32	ND	N/A
Aph1 $\beta$	aph-1 homolog b, $\gamma$ -secretase subunit $\beta$ -1.33	0.33	ND	N/A	
Cd14	cluster of differentiation 14	1.65	0.14	0.09	0.17
Cd68	cluster of differentiation 68 (lamp 4)	1.42	0.02	ND	N/A
Itgav	integrin subunit $\alpha$ -V	1.02	0.92	0.70	0.96
Itgb3	integrin subunit $\beta$ -3	1.08	0.71	ND	N/A
Itgb5	integrin subunit $\beta$ -5	-1.17	0.11	ND	N/A
Mertk	MER proto-oncogene tyrosine kinase -1.54	0.11	ND	N/A	
Mfge8	milk-fat globule EGF factor 8	-1.22	0.13	1.06	0.88

TABLE 2 (Continued)

Gene symbol	Gene description	mRNA null/wild type <sup>†</sup>	adj. p value	Protein null/wild type <sup>†</sup>	adj. p value
Rac1	rac family small GTPase 1	1.14	0.11	<b>6.74</b>	<b>3.42E-05</b>
Thbs1	thrombospondin	<b>4.83</b>	<b>0.02</b>	ND	N/A
Extrinsic Apoptosis					
Fadd	Fas-associated by death domain	-1.12	0.48	5.60	0.36
Ikkkb	Inhib, of nuclear factor $\kappa$ B kinase subunit $\beta$	1.02	0.84	16.75	0.12
Tnfrsf12a	TNF receptor family member 12a (TweakR)	<b>2.67</b>	<b>0.005</b>	ND	N/A
Casp 3	Caspase 3	<b>-1.74</b>	<b>0.005</b>	<b>0.115</b>	<b>0.004</b>
Casp 6	Caspase 6	-1.02	0.63	1.23	0.78
Casp 8	Caspase 8	1.08	0.48	<b>&gt;100</b>	<b>5.80E-17</b>
Misplacement of survivin					
Birc5	baculoviral IAP repeat cont. 5 (survivin)	2.90	0.15	ND	N/A
Slc5a8	solute carrier family 5, member 8	<b>9.75</b>	<b>0.012</b>	ND	N/A

<sup>†</sup>Significant fold changes  $\geq \pm 1.5$  (adj. p value  $\leq 0.05$ ) for both mRNA and protein (red), mRNA only (purple), protein only (green).

<sup>‡</sup>ND, Not detected; N/A, Not applicable.

<sup>§</sup>The ratio cannot be calculated as the protein was only detected in one genotype.

had detectable levels (1.3 nmol/ $\mu$ g lipid) (Figure S5B,C). Oxidative damage to proteins was assessed by immunoblot of post-nuclear supernatant samples from *Btn1a1*<sup>+/+</sup> and *Btn1a1*<sup>-/-</sup> mice using specific antibodies to probe for the presence of carbonyl groups,<sup>45</sup> or 3-nitrotyrosine residues.<sup>46</sup> In neither case were there any significant differences between wild type and knockout samples (Figure S5D-G).

### 3.4 | Lactation is maintained in *Btn1a1*<sup>-/-</sup> mice by continued epithelial cell renewal

Besides, cell injury and cell death pathways, the RNAseq and proteomics data indicated upregulation of DNA synthesis and mitosis in *Btn1a1*<sup>-/-</sup> mice during lactation. Cell renewal and regeneration of the mammary epithelium would explain how lactation can be maintained for 3 weeks in many *Btn1a1*<sup>-/-</sup> animals,<sup>13</sup> despite a high incidence of cell damage and death. To confirm cell renewal, tissue sections of all three genotypes were stained with a commercial antibody to Ki67, a protein that is only expressed in the nucleus of actively dividing cells.<sup>47</sup> Ki67 was largely absent from wild type cells, was present in some *Btn1a1*<sup>+/+</sup> cells but substantially more in *Btn1a1*<sup>-/-</sup> mice (Figure 7A). Embryonic day-18 mouse tissue, in which there is extensive mitosis served as a positive control for the commercial Ki67 antibody (Figure 7B). Quantitation of the Ki67 distribution in all three genotypes (five mice/

genotype) confirmed a statistically significant number of mitotic cells in *Btn1a1*<sup>-/-</sup> mice (10% of total cells) compared with wild type controls (Figure 7C; Table S4).

## 4 | DISCUSSION

The large increase of Xdh protein in *Btn1a1*<sup>-/-</sup> mice with no significant change in mRNA levels, provides further evidence that Btn1a1 and Xdh are functionally linked in the secretion of LDs. Build up in cytoplasmic Xdh is most probably due to disrupted lipid metabolism (Figure S1D, Excel Spreadsheet 11) and dysregulated secretion of Xdh with unstable LDs in the absence of its binding partner. However, because *Btn1a1* in this KO2 mouse line is not completely ablated, the fragments of Btn1a1 identified in knockout cells (Figure A2) may have interfered with the budding of LDs by some secondary mechanism. This possibility is unlikely as LD secretion is not inhibited in *Btn1a1*<sup>+/+</sup> mice, in which at least half of the Btn1a1 is degraded (Figure A3). Furthermore, a previous Btn1a1-deficient mouse line (KO1) had a similar phenotype with respect to cell damage and enlarged LDs but the truncated Btn1a1 expressed was incorporated into membranes with no evidence of protein degradation.<sup>13</sup>

Despite the large increase in Xdh protein there was little evidence for changes in the levels of the respective

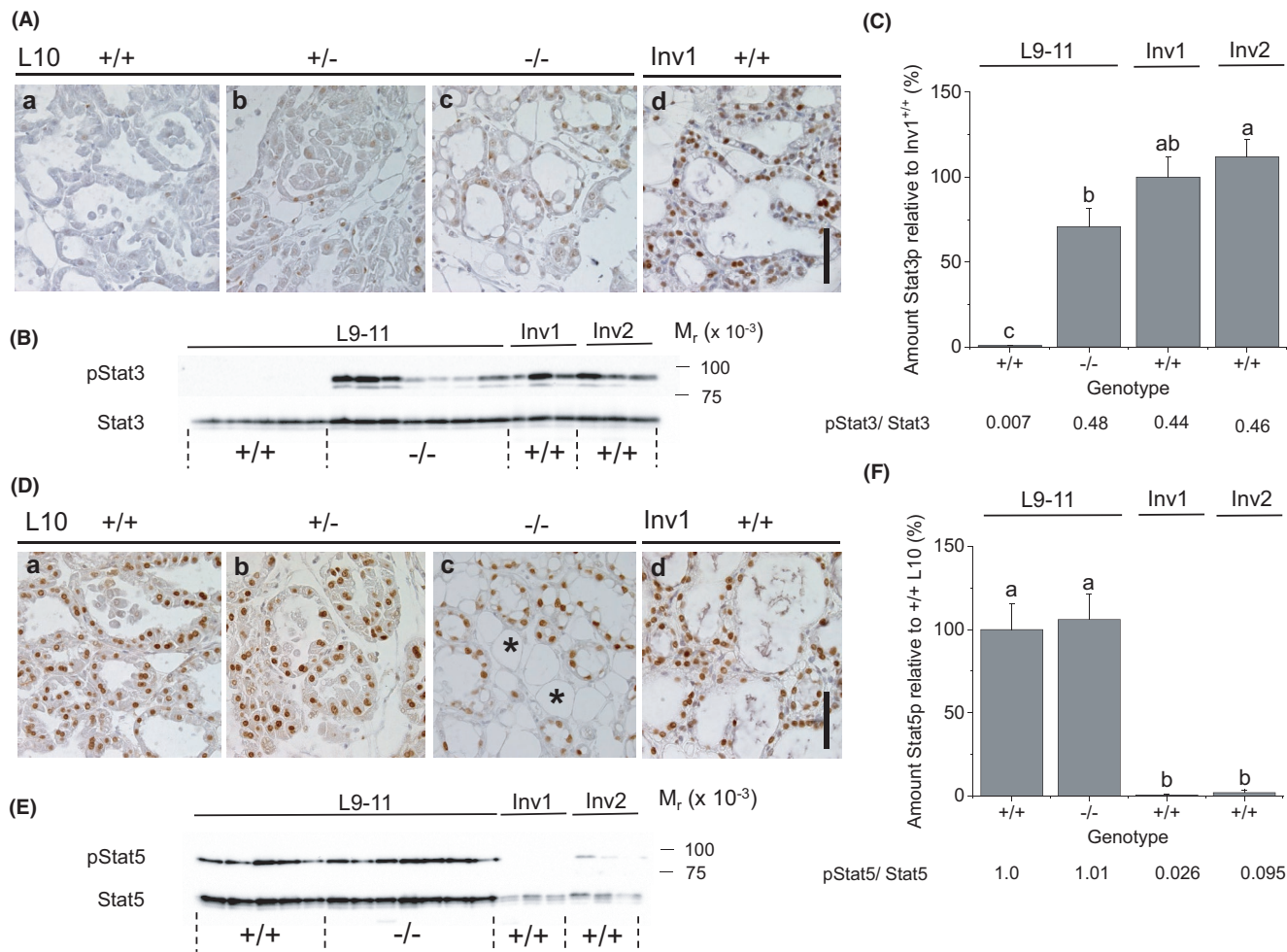


**FIGURE 5** Expression and phosphorylation of Stat3 and Stat5. (A–C) Stat3 is phosphorylated and accumulates in the nucleus at peak lactation (day 10) in *Btn1a1*<sup>-/-</sup> mice. (A) pStat3 was detected in sections of paraffin-embedded mammary gland from (a) *Btn1a1*<sup>+/+</sup>, (b) *Btn1a1*<sup>+/-</sup>, and (c) *Btn1a1*<sup>-/-</sup> (lactation day 10, L10) and (d) *Btn1a1*<sup>+/+</sup> (involution day 1, Inv1) mice by the ABC VectorStain procedure as described in Materials and Methods. Representative examples of each genotype (3–6 sections each from three mice/genotype). Bar 100  $\mu$ m. (B) Expression of Stat3 and phosphorylated Stat3 monitored by immunoblot of THs (60  $\mu$ g protein/lane; 10% polyacrylamide) from 5 *Btn1a1*<sup>+/+</sup>, 7 *Btn1a1*<sup>-/-</sup> mice at lactation days 9–11 (L9–11) and three each, *Btn1a1*<sup>+/+</sup> mice at involution days 1 and 2 (Inv1 and Inv2, respectively). pStat3 was detected with a 1000-fold dilution of rabbit anti-peptide-Y705 antibody, followed by a 1000-fold dilution of goat anti-rabbit IgG-HRP. Total Stat3 was detected on the same stripped blot with a 1000-fold dilution of rabbit anti-C-terminal Stat3-peptide antibody, followed by a 1000-fold dilution of goat anti-rabbit IgG-HRP. (C) Triplicate blots as in B were quantified and data normalized to the amount of pStat3 in the Inv1 samples (set to 100%). pStat3/Stat3 ratios are given below the graph. Columns with different letters are statistically different from each other. Means  $\pm$  SEM,  $p < 0.05$ , F-test (ANOVA). (D–F) Stat5 is phosphorylated and accumulates in the nucleus at peak lactation (day 10) in *Btn1a1*<sup>+/+</sup>, *Btn1a1*<sup>+/-</sup>, and *Btn1a1*<sup>-/-</sup> mice. (D) pStat5 was detected in sections of paraffin-embedded mammary gland as in A–C. Representative examples of each genotype (3–5 sections each from three mice/genotype). Alveoli denuded of epithelial cells (alveolar “ghosts”) discussed in the text are marked by asterisks in the knockout sample. Bar 100  $\mu$ m. (E) Expression of Stat5 and phosphorylated Stat5 monitored by immunoblot of THs as in B above. Phosphorylated Stat5 (pStat5) was detected with a 1000-fold dilution of rabbit anti-peptide-Y694 antibody, followed by a 1000-fold dilution of goat anti-rabbit IgG-HRP. Total Stat5 was detected on the same stripped blot with a 1000-fold dilution of rabbit anti-peptide Stat5 antibody, followed by a 1000-fold dilution of goat anti-rabbit IgG-HRP. (F) Duplicate blots as in E were quantified and data normalized to the amount of pStat5 in the *Btn1a1*<sup>+/+</sup> L10 samples (set to 100%). pStat5/Stat5 ratios are given below the graph. Columns with different letters are statistically different from each other. Means  $\pm$  SEM,  $p < 0.05$ , F-test (ANOVA)

mRNAs and proteins associated with purine metabolism, with the possible exception of some enzymes essential for AMP and GMP synthesis (Excel Spreadsheet 18). Notably, there were no significant changes in adenine

phosphoribosyltransferase and hypoxanthine guanine phosphoribosyltransferase, the two enzymes required for “rescue” of hypoxanthine, a substrate of Xdh, in the purine “salvage pathway”. On the other hand, there was

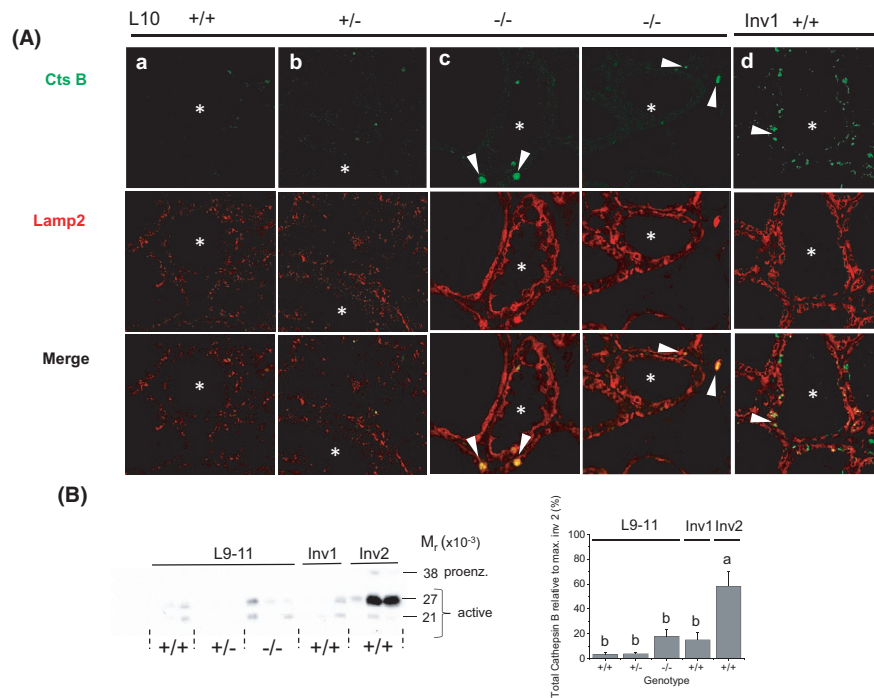


**FIGURE 6** Cathepsin B distribution in *Btn1a1*<sup>+/+</sup>, *Btn1a1*<sup>+/-</sup>, and *Btn1a1*<sup>-/-</sup> mammary cells at peak lactation (day 10). (A) Sections of paraffin-embedded mammary gland from (a) *Btn1a1*<sup>+/+</sup>, (b) *Btn1a1*<sup>+/-</sup>, and (c) two examples, *Btn1a1*<sup>-/-</sup> (lactation day 10, L10) and (d) *Btn1a1*<sup>+/+</sup> (involution day 1, Inv1) mice were double-labeled with antibodies to cathepsin B (Cts B) (Thermo) and lamp2 as described in Materials and Methods. Representative examples of each genotype (2–3 sections each from 3 mice/genotype) are shown for cathepsin B, lamp2 and the merged images. Note cathepsin B-positive structures in *Btn1a1*<sup>-/-</sup> and *Btn1a1*<sup>+/+</sup> Inv1 mice (arrowheads). (B) Expression of cathepsin B monitored by immunoblot of THs (75  $\mu$ g protein/lane; 10% polyacrylamide) from *Btn1a1*<sup>+/+</sup>, *Btn1a1*<sup>+/-</sup>, *Btn1a1*<sup>-/-</sup> mice at lactation days 9–11 (L9-11) (three mice/genotype) and three each, *Btn1a1*<sup>+/+</sup> mice at involution days 1 and 2 (Inv1 and Inv 2, respectively). Cathepsin B was detected with a 1000-fold dilution of monoclonal rabbit anti-(human cathepsin B) (Abcam), followed by a 3,000-fold dilution of goat anti-(rabbit IgG)-HRP. Pro-cathepsin B and active forms are indicated to the right of the figure. Total cathepsin B was quantified on four blots to generate duplicate data for seven *Btn1a1*<sup>+/+</sup>, five *Btn1a1*<sup>+/-</sup>, and six *Btn1a1*<sup>-/-</sup> mice on lactation days 9–11 (L9-11) and quadruplicate data for three mice, each on days 1 and 2 of involution (Inv1, and Inv2, respectively). Amounts of cathepsin B were normalized to the most positive Inv 2 *Btn1a1*<sup>+/+</sup> mouse (set to 100%) in the graph to the right of the blot. Columns with different letters are statistically different from each other. Means  $\pm$  SEM,  $p < 0.05$ , F-test (ANOVA). Brightness in all micrographs was increased by 20% because of low fluorescence signals in the wild type and heterozygote samples. Asterisks, alveolar luminae, Bars 20  $\mu$ m

significant downregulation of pathways associated with amino acid metabolism (Excel Spreadsheets 4,6,7), enhanced adenosine receptor signaling (Excel Spreadsheet 9), nitrogen compound metabolism (Excel Spreadsheet 12), and purine nucleotide/ribonucleotide binding (Excel Spreadsheet 14). Metabolomic analysis of differences between wild type and null mice would help establish the significance of many of these changes.

In a broader context, the *Btn1a1*<sup>-/-</sup> KO2 mouse presents a useful model for exploring the regulation of cell death and renewal during an established lactation as an alternative to the established practice of acutely inducing cell death by weaning at peak lactation.<sup>48</sup> As discussed below, accumulation of large cytoplasmic LDs and cell damage initiates multiple pathways that differ from the currently accepted paradigm.

Cell death in wild type mice occurs in two stages, an initial Phase 1 that is reversible if the milking stimulus

is restored, and a second irreversible Phase 2, during which the gland is permanently remodeled.<sup>49,50</sup> Phase 1 is characterized by acute phase,<sup>51-53</sup> and unfolded protein responses,<sup>54</sup> autophagy,<sup>54,55</sup> and the efferocytosis<sup>55,56</sup> of lysosome-digested cells. The initial trigger is assumed to be the Lif-induced phosphorylation of Stat3,<sup>40,41,57</sup> although over the past 25 years many other pathways have been invoked.<sup>58-62</sup> Phase 2 is dominated by matrix remodeling through the action of metalloproteinases (Mmps) and a wound healing response mediated by M2-macrophages. Oncostatin M (Osm) replaces Lif as the principal ligand maintaining Stat3 levels.<sup>53,63</sup>

Involution in lactating *Btn1a1*<sup>-/-</sup> mice progresses through at least the first half of Phase 1, possibly triggered by the fusion of unstable milk-LDs, which block luminal spaces in local areas of the gland.<sup>13</sup> In wild type cells, increased milk pressure precipitates stretch-induced downregulation of the apical Ca<sup>2+</sup> channel, Atp2b2 (PMCA2) and an

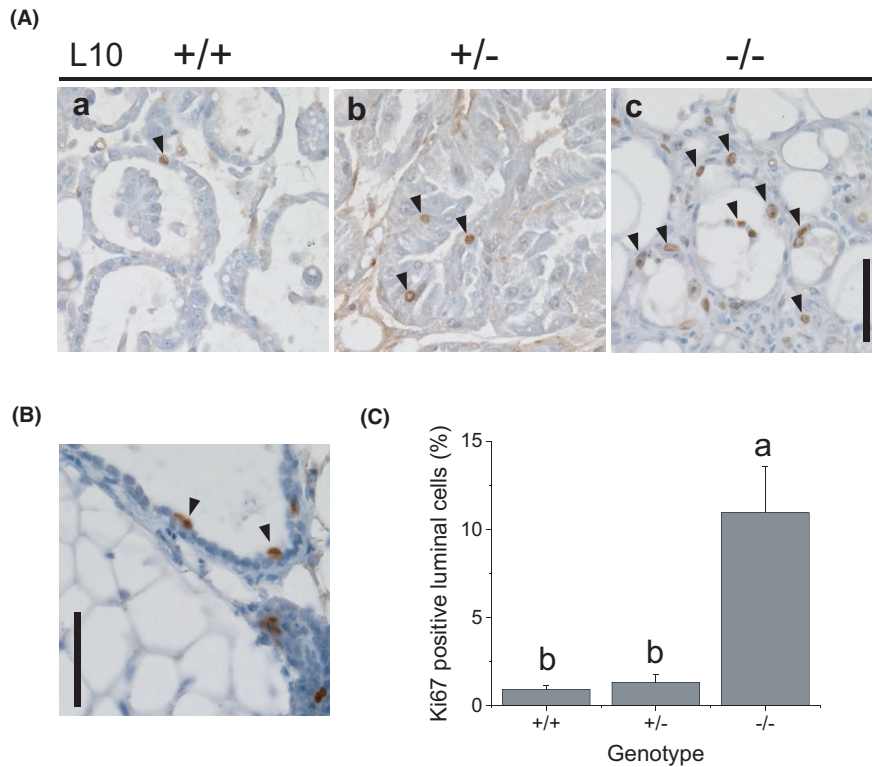


**FIGURE 7** The number (%) of mitotic epithelial cells increases at peak lactation in *Btn1a1*<sup>-/-</sup> mice. (A) Ki67 was detected in sections of paraffin-embedded mammary gland from (a) *Btn1a1*<sup>+/+</sup>, (b) *Btn1a1*<sup>+/-</sup>, and (c) *Btn1a1*<sup>-/-</sup> (lactation day 10, L10) by the ABC VectorStain procedure, as described in Materials and Methods. The number of Ki67-positive nuclei was significantly increased in luminal *Btn1a1*<sup>-/-</sup> cells compared with cells in *Btn1a1*<sup>+/+</sup> and *Btn1a1*<sup>+/-</sup> mice (arrowheads). Representative examples of each genotype (4–6 sections, each from five mice/genotype). Bar 100  $\mu$ m. (B) Section of embryonic day-18 mouse mammary gland used as a positive control for Ki67 staining (1 of 5 examples). (C) Comparison of the number (%) of Ki67-positive luminal cells at day 10 of lactation in *Btn1a1*<sup>+/+</sup>, *Btn1a1*<sup>+/-</sup>, and *Btn1a1*<sup>-/-</sup> mice (respective number of cells counted/genotype, 2,979, 2,529, and 1,418). Columns with different letters are statistically different from each other. Means  $\pm$  SEM,  $p < 0.05$ , F-test (ANOVA)

increase in cytoplasmic Ca<sup>2+</sup> levels.<sup>64–66</sup> In *Btn1a1* null cells, marginal decreases in mRNA for Atp2b2 and the secretory pathway Ca<sup>2+</sup> channel (Atp2c2) (Table 2) are also in line with this possibility. Another potential trigger is oxidative damage caused by excess Xdh in the cytoplasm (Figure 1), although there was little evidence for this from analysis of tissue and milk samples (Figure S5). Judging from both the RNAseq and proteomic data this lack of oxidative damage was not due to a rise in protective enzymes, such as catalase and superoxide dismutase (Excel Spreadsheet 18).

As in wild type animals, Phase 1 in lactating *Btn1a1*<sup>-/-</sup> mice is characterized by a significant increase in *Lif* and an acute phase response (Table 2, Figure S3B). *Lif* mRNA is upregulated 7.27-fold (adj.  $p$  value 0.01) and *Stat3* mRNA is marginally increased (1.42-fold, adj.  $p$  value 0.04). *Stat3* is phosphorylated and translocated into the nucleus (Figure 5A–C), despite potential redox interference in *Stat3* phosphorylation<sup>67</sup> by increased amounts of Xdh. In addition, mRNA encoding *Timp1*, which suppresses matrix degradation is increased almost twofold (Table 2). The possibility that inflammation is initiated by

Il-6 signaling, as in the liver (Figure 3B,F,G) is unlikely in *Btn1a1*<sup>-/-</sup> mice, because *Stat3* activation is independent of Il-6 in mammary cells.<sup>41,68</sup>

Modulation of the NF $\kappa$ B pathway, which mediates the inflammatory response<sup>61</sup> may be significant in *Btn1a1*<sup>-/-</sup> mice as there were increases in NF $\kappa$ B2 and *Ikbkb* protein, and mRNA for the coactivator, *Bcl3*. Also, there was evidence for activation of the TGF- $\beta$ 3/Smad pathway, which modulates growth arrest and/or apoptosis in concert with *Pkb/Akt*<sup>59,69</sup> and may regulate the activity of *Stat3*. TGF- $\beta$ 3 mRNA was unchanged but there were elevations in mRNA for the effector, *Klf10* (1.64, adj.  $p$  value 0.04) and for *Smad3* protein (85.2-fold, adj.  $p$  value 0.004). However, there was no significant change in mRNA for *C/ebp $\delta$*  (1.15-fold, adj.  $p$  value 0.59), which increases 100-fold within the first 12 h in involuting wild type cells and suppresses *cyclin D1*, a key regulator of the cell cycle.<sup>61,70</sup> This latter result is consistent with the ongoing mitosis evident in lactating *Btn1a1* null animals.

In contrast to the forced weaning model, there were significant differences in final modes of execution. In

involving wild type mice, the unfolded protein response and autophagy initially serve as survival mechanisms as metabolism is slowed and cells reflux lipids and amino acids in an attempt to rebuild cellular structures.<sup>54</sup> Autophagy precedes, and is essential for the initiation of efferocytosis, in the event that cell survival falters.<sup>55</sup> Surprisingly, there was little evidence of an unfolded protein response in *Btn1a1* null mice (Table 2) but several autophagy proteins were upregulated, including Atg4b, Atg 7, and Map11c3b (LC3 $\beta$ ) (Table 2, Figure S3A). Nevertheless, beclin (Becn1), which is a key initiator of autophagy,<sup>55</sup> was unchanged. Limited activation of autophagy may have limited the onset of efferocytosis, as there was no change in several major players, including  $\gamma$ -secretase (subunits, Aph1 $\alpha$  and  $\beta$ ), the vitronectin receptor (integrin subunits, Itg $\alpha$ V, and Itg $\beta$ 3) and Mfg-e8 (Table 2). However, mRNA for thrombospondin, which may mediate cell-to-cell contact was significantly elevated 4.83-fold (adj. *p* value 0.02) and rac1 protein, which reorganizes the actin cytoskeleton during the initial stages of efferocytosis was increased by 6.74-fold (adj. *p* value 3.42E-05). Thus in null mice, autophagy may primarily function as a survival mechanism, which limits the onset of efferocytosis.

Evidence for cell death by the currently accepted lysosomal lysis pathway was ambiguous.<sup>43,71</sup> On the one hand, a small number of cathepsin B/ lamp2 positive structures (presumed lysosomes) were detected in null mice at peak lactation (Figure 6A,c) along with a correspondingly modest increase in the amount of cathepsin B estimated by immunoblot (Figure 6B). Furthermore, the widespread distribution of lamp2 in apical regions indicated disruption of membrane recycling between the plasma membrane and endosomal/lysosomal system. On the other hand, cathepsin B staining was coincident with lamp2 in null mice (arrowheads, Figure 6A,c), whereas in the wild type involuting controls the two staining patterns diverged (Figure 6A,d). Such divergence is seen as a hallmark of lysosomal lysis in wild type animals,<sup>43</sup> thus suggesting that cathepsin B expression was at an early stage of Phase 1 involution in *Btn1a1*<sup>-/-</sup> mice. In addition, there was little change in the expression of 11 cathepsins, with the exception of cathepsin H and S protein, and cathepsin Z mRNA. Most significantly, *Serpina3g* (*Spi2a*), which inhibits many cathepsins was unchanged in *Btn1a1*<sup>-/-</sup> mice (Table 2), whereas there is a > 250-fold decrease during lysosomal-mediated involution in wild type cells.<sup>43</sup> Death by lysosomal lysis in null cells at peak lactation may be impeded by their inability to endocytose the large unstable LDs typical of knockout animals (Figure S4), thus preventing the generation of membrane permeabilizing fatty acids.<sup>71</sup>

Unlike in wild type cells,<sup>43</sup> the classical extrinsic apoptosis pathway is a possible mode of cell death

(Figure S6). First, mRNA levels were elevated in null cells for the cell surface death receptor, *Tnfrsf12a*, as was protein for the NF- $\kappa$ B inhibitor, *Ikbkb* (Table 2), both of which promote the extrinsic pathway.<sup>72</sup> Second, caspase 8 protein, which activates caspase 3, was only detected in *Btn1a1*<sup>-/-</sup> cells. Although the key executioner, caspase 3 was significantly downregulated at both the mRNA and protein levels (Table 2), there was clear immunohistochemical evidence for active caspase 3 (Figure 4C,c,d) and DNA laddering in 10% of the secretory cells at day 10 of lactation (Figure 4A, B). The intrinsic mitochondrial pathway is a less likely route as most pro- and anti-apoptotic members of the Bcl-2 family were unchanged at either the mRNA or protein levels, with the exception of *Bcl2l13* (Figure S6).

One other cell death route deserves mention. Expression of mRNA for the Na<sup>+</sup>-coupled monocarboxylate solute transporter, *Slc5a8*, was elevated 9.75-fold (adj. *p* value 0.016) in *Btn1a1*<sup>-/-</sup> mice (Table 2). *Slc5a8* promotes apoptosis by interacting with *Birc5* (survivin), a member of the inhibitor of apoptosis (IAP) family.<sup>73</sup> *Birc5*, in acetylated form, is located in the nucleus, where it regulates cytokinesis and inhibits the transactivation of *Stat3* target genes.<sup>74</sup> *Slc5a8* binds to *Birc5* and misdirects it to the plasma membrane, where it is sequestered, thus increasing *Stat3* and caspase activity.<sup>73</sup> Increased expression of *Slc5a8* may therefore serve as an adjunct death mechanism in *Btn1a1* null animals.

The irreversible Phase 2 of involution was not significant in lactating *Btn1a1* null mice as neither mRNA nor protein was detected for *Osm* or its downstream effector, chitinase-3-like 1 (*Chi3l1*) (Table 2). Furthermore, basement membrane structures remained relatively intact (see, e.g., alveolar “ghosts” in the *Btn1a1*<sup>-/-</sup> sample in Figure 5D,c) and *Mmp12* was the only metalloproteinase of nine that was marginally increased 1.61-fold at the mRNA level (adj. *p* value 0.02). However, there was a significant increase in mRNA for arginase 1 (*arg1*) (4.81-fold, adj. *p* value 0.011), which is a key marker for wound healing responses mediated through M2-macrophages.<sup>75</sup> Phase 2 in null mice is most probably prevented by continued exposure of the glands to lactogenic hormones.<sup>50</sup>

In wild type mice, less than 0.4% of milk-secreting cells are estimated to die on a daily basis,<sup>76</sup> whereas approx. 10% of the nuclei in *Btn1a1* null cells were TUNEL-positive on a single day at peak lactation (Figure 4). Evidence for continued cell division against a background of arrested and dying cells is clear from the IPA and GSEA analysis of the RNAseq data. Many key molecules of the cell cycle and DNA replication were upregulated at the mRNA level including cyclins, cyclin-dependent kinase 1 (*Cdc2*), and *Mcm* components of the pre-replication complex (Table 3). However,

it is unlikely that cell numbers are maintained at wild type levels throughout the lactation cycle because litter weight gains (as an indirect measure of milk yield) are depressed by 20%–40% in knockout animals.<sup>13</sup> Presumably, nascent secretory cells develop from pre-existing luminal stem cells.<sup>77</sup> The interesting possibility that alveolar binucleate cells might be a facile source of new cells, is contra-indicated by the elevated expression of mRNA encoding Aurka and Plk1 (Table 3). Both are kinases that generate binucleate cells by blocking cytokinesis in late pregnancy in wild type mice.<sup>78</sup>

In summary, the death of milk-secreting epithelial cells in *Btn1a1*<sup>-/-</sup> mice is multi-factorial, most probably

triggered by lipid accumulation in local areas of the gland, initiated by Lif-induced phosphorylation of Stat3 and accompanied by an acute phase response. Cell death may proceed through the actions of caspases 8 and 3, fragmentation of nuclear DNA, and possibly through autophagy and lysosomal lysis. Also, mis-targeting of Birc5 by Slc5a8 may play a role. Elements of the extracellular matrix are maintained, unlike the irreversible remodeling that occurs during Phase 2 of involution in wild type mice. The lack of a single cell death pathway is most likely because localized build-up of luminal fat triggered a heterogeneous response in null animals, which was revealed by principal component and GSEA analysis (Figure 2A,B,

**TABLE 3** Fold change in expression of selected mRNAs associated with the cell cycle in the lactating mammary glands of *Btn1a1*<sup>-/-</sup> compared with *Btn1a1*<sup>+/+</sup> mice

Gene symbol	Gene description	mRNA null/wild type <sup>†</sup>	adj. p value
Aurka	Aurora kinase A	<b>2.19</b>	<b>0.05</b>
Ccna2	Cyclin A2	<b>4.65</b>	<b>0.05</b>
Ccnb1	Cyclin B1	5.90	0.07
Ccnb2	Cyclin B2	2.63	0.09
Ccnd1	Cyclin D1	-1.03	0.93
Ccne1	Cyclin E1	1.75	0.14
Ccne2	Cyclin E2	2.00	0.14
Cdc7	Cell division cycle 7	2.03	0.06
Cdc20	Cell division cycle 20	3.62	0.10
Cdk1	Cyclin dependent kinase 1 (Cdc2)	<b>3.80</b>	<b>0.05</b>
Cdk2	Cyclin dependent kinase 2	1.10	0.56
Cdk4	Cyclin dependent kinase 4	1.13	0.22
Cdk6	Cyclin dependent kinase 6	1.16	0.43
Cdkn1a	Cyclin dependent kinase inhibitor 1a (p21)	1.33	0.39
E2f1	E2F transcription factor 1	1.35	0.11
E2f2	E2F transcription factor 2	1.26	0.55
Fos	Fos proto-oncogene, AP1 subunit	<b>2.25</b>	<b>0.01</b>
Jun	Jun proto-oncogene, AP1 subunit (c-Jun)	<b>2.55</b>	<b>0.006</b>
JunB	JunB proto-oncogene, AP1 subunit	<b>2.48</b>	<b>0.02</b>
JunD	JunD proto-oncogene, AP1 subunit	1.07	0.64
Mcm2	MCM component 2	<b>1.92</b>	<b>0.03</b>
Mcm4	MCM component 4	<b>2.12</b>	<b>0.03</b>
Mcm5	MCM component 5	3.34	0.07
Mcm6	MCM component 6	<b>2.47</b>	<b>0.03</b>
Mcm7	MCM component 7	1.52	0.17
Plk1	Polo-like kinase 1	2.39	0.12
Rb1	Rb transcriptional corepressor 1	1.14	0.42
Rpa1	Replication protein A1	1.01	0.91
Sfn	Stratifin, (14-3-3-σ)	<b>1.92</b>	<b>0.005</b>

<sup>†</sup>Significant fold changes  $\geq \pm 1.5$  (adj. p value  $\leq 0.05$ ) highlighted in purple.

Figure S1) and pStat3 and cathepsin B immunoblots (Figures 5B, 6B). A more refined synthesis would require analysis of temporal changes in single cells, as recently described for the RNAseq analysis of cells isolated from human milk.<sup>79</sup>

This analysis illustrates the plasticity and resilience of the mammary epithelium to physical insults and the importance of functional Btn1a1 expression for maintenance of terminally differentiated secretory cells. Clinical studies of BTN1A1 and XDH expression and milk composition might reveal some of the underlying reasons that lactation fails in 5% of breast-feeding mothers.<sup>80</sup> In this context, purine, pyrimidine, and amino acids are significantly raised in the milk of obese mothers, who frequently fail to sustain adequate milk production.<sup>81,82</sup> Outside the realms of mammary gland biology, these findings may have significance for the modulation and function of immune cells, given the role that XDH plays in innate immunity<sup>83</sup> and the multiple immune functions of the BTN family, including BTN1A1.<sup>4,84</sup>

#### ACKNOWLEDGMENTS

The authors thank Dr. Toren Finkel (University of Pittsburgh, PA) for the *Xdh*<sup>-/-</sup> mouse line and Jinling Xu (University of Maryland), Dr. Yeap Ng, Sherry Rausch, and Samri Gebre (National Cancer Institute, NIH) for animal management and care. Dr. Bao Tran and Jyoti Shetty conducted the RNAseq analysis at the Illumina Sequencing Facility (Frederick National Laboratory for Cancer Research, MD) and Dr. Maggie Cam (National Cancer Institute, NIH) provided advice on bioinformatics analysis. This research was supported, in part, by the Intramural Research Program of the NIH, National Cancer Institute, Center for Cancer Research and funded by grants to JJW from the NIH, R01HD06248 and R01HD100468, and to IHM from the NIH, R01HD048588-01A1, the U.S. Department of Agriculture (NRI 0003264 and 2005-04637), and the Maryland Agricultural Experiment Station.

#### CONFLICT OF INTEREST

The authors have no conflicts of interest to declare.

#### AUTHOR CONTRIBUTIONS

JJ completed the experiments described in Figures 1, 4-7 (histology). AKGK assisted with the immunoblotting data in Figure 1, crossed *Btn1a1*<sup>+/-</sup> and *Xdh*<sup>+/-</sup> mouse lines to generate mouse lines used for Figure 1D,E, conducted *Xdh* (oxidase) assays, the RT-PCR analysis in the Appendix and analyzed all data for statistical significance. The RNAseq data were configured and analyzed by TJM and the proteomic analysis conducted by LMJ and JCD. IHM conceived and supervised the project together with

JJW and RW, conducted the ROS assays in Figure S5, the immunoblots in Figures 5, 6 and A3, and wrote an initial draft of the text.

#### ORCID

Ian H. Mather  <https://orcid.org/0000-0002-9351-1381>

#### REFERENCES

1. Franke WW, Heid HW, Grund C, et al. Antibodies to the major insoluble milk fat globule membrane-associated protein: specific location in apical regions of lactating epithelial cells. *J Cell Biol.* 1981;89:485-494.
2. Jack LJW, Mather IH. Cloning and analysis of cDNA encoding bovine butyrophilin, an apical glycoprotein expressed in mammary tissue and secreted in association with the milk-fat globule membrane during lactation. *J Biol Chem.* 1990;265:14481-14486.
3. Heid HW, Winter S, Bruder G, Keenan TW, Jarasch E-D. Butyrophilin, an apical plasma membrane-associated glycoprotein characteristic of lactating mammary glands of diverse species. *Biochim Biophys Acta.* 1983;728:228-238.
4. Arnett HA, Viney JL. Immune modulation by butyrophilins. *Nature Rev Immunol.* 2014;14:559-569.
5. Tazi-Ahnini R, Henry J, Offer C, Bouissou-Bouchouata C, Mather IH, Pontarotti P. Cloning, localization, and structure of new members of the butyrophilin gene family in the juxtatelomeric region of the major histocompatibility complex. *Immunogenetics.* 1997;47:55-63.
6. Sandstrom A, Peigne C-M, Leger A, et al. The intracellular B30.2 Domain of butyrophilin 3A1 binds phosphoantigens to mediate activation of human Vγ9Vδ2 T cells. *Immunity.* 2014;40:490-500.
7. Jeong J, Rao AU, Xu J, et al. The PRY/SRY/B30.2 domain of butyrophilin 1A1 (BTN1A1) binds to xanthine oxidoreductase: Implications for the function of BTN1A1 in the mammary gland and other tissues. *J Biol Chem.* 2009;284:22444-22456.
8. Woo JS, Suh HY, Park SY, Oh BH. Structural basis for protein recognition by B30.2/SPRY domains. *Mol Cell.* 2006;24:967-976.
9. Rhodes DA, de Bono B, Trowsdale J. Relationship between SPRY and B30.2 protein domains. Evolution of a component of immune defence? *Immunology.* 2005;116:411-417.
10. Laing KJ, Purcell MK, Winton JR, Hansen JD. A genomic view of the NOD-like receptor family in teleost fish: identification of a novel NLR subfamily in zebrafish. *BMC Evol Biol.* 2008;8:42.
11. Rigau M, Ostrouska S, Fulford TS, et al. Butyrophilin 2A1 is essential for phosphoantigen reactivity by γδ T cells. *Science.* 2020;367:eaay5516.
12. Masedunskas A, Chen Y, Stussman R, Weigert R, Mather IH. Kinetics of milk lipid droplet transport, growth, and secretion revealed by intravital imaging: lipid droplet release is intermittently stimulated by oxytocin. *Mol Biol Cell.* 2017;28:935-946.
13. Ogg SL, Weldon AK, Dobbie L, Smith AJH, Mather IH. Expression of butyrophilin (Bt1a1) in lactating mammary gland is essential for the regulated secretion of milk-lipid droplets. *Proc Natl Acad Sci USA.* 2004;101:10084-10089.
14. Mather IH, Keenan TW. Origin and secretion of milk lipids. *J Mamm Gland Biol Neopl.* 1998;3:259-273.

15. Monks J, Dzieciatkowska M, Bales ES, Orlicky DJ, Wright RM, McManaman JL. Xanthine oxidoreductase mediates membrane docking of milk-lipid droplets but is not essential for apocrine lipid secretion. *J Physiol*. 2016;594(20):5899-5921.
16. Vorbach C, Scriven A, Capecchi MR. The housekeeping gene xanthine oxidoreductase is necessary for milk fat droplet enveloping and secretion: gene sharing in the lactating mammary gland. *Genes Develop*. 2002;16:3223-3235.
17. Wang W, Lv N, Zhang S, et al. Cidea is an essential transcriptional coactivator regulating mammary gland secretion of milk lipids. *Nature Med*. 2012;18:235-243.
18. Zhao L, Ke H, Xu H, et al. TDP-43 facilitates milk lipid secretion by posttranscriptional regulation of Btn1a1 and Xdh. *Nature Commun*. 2020;11:Article 341.
19. Ohtsubo T, Rovira II, Starost MF, Liu C, Finkel T. Xanthine oxidoreductase is an endogenous regulator of cyclooxygenase-2. *Circ Res*. 2004;95:1118-1124.
20. Towbin H, Staehelin T, Gordon J. Electrophoretic transfer of proteins from polyacrylamide gels to nitrocellulose sheets: procedure and some applications. *Proc Natl Acad Sci USA*. 1979;76:4350-4354.
21. Laemmli UK. Cleavage of structural proteins during the assembly of the head of bacteriophage T<sub>4</sub>. *Nature*. 1970;227:680-685.
22. Warburton MJ, Mitchell D, Ormerod EJ, Rudland P. Distribution of myoepithelial cells and basement membrane proteins in the resting, pregnant, lactating and involuting rat mammary gland. *J Histochem Cytochem*. 1982;30:667-676.
23. Foley J, Dann P, Hong J, et al. Parathyroid hormone-related protein maintains mammary epithelial fate and triggers nipple skin differentiation during embryonic breast development. *Development*. 2001;128:513-525.
24. Franke WW, Krien S, Brown RM. Simultaneous glutaraldehyde-osmium tetroxide fixation with postosmication. An improved fixation procedure for electron microscopy of plant and animal cells. *Histochemie*. 1969;19:162-164.
25. Gavrieli Y, Sherman Y, Ben-Sasson SA. Identification of programmed cell death in situ via specific labeling of nuclear DNA fragmentation. *J Cell Biol*. 1992;119:493-501.
26. Martin M. Cutadapt removes adapter sequences from high-throughput sequencing reads. *EMBnet journal*. 2011;17(1):10-12.
27. Dobin A, Davis CA, Schlesinger F, et al. STAR: ultrafast universal RNA-seq aligner. *Bioinformatics*. 2013;29:15-21.
28. Leek JT, Scharpf RB, Bravo HC, et al. Tackling the widespread and critical impact of batch effects in high-throughput data. *Nat Rev Genetics*. 2010;11:733-739.
29. Perez-Riverol Y, Csordas A, Bai J, et al. The PRIDE database and related tools and resources in 2019: improving support for quantification data. *Nucleic Acids Res*. 2019;47(D1):D442-D450.
30. Li B, Dewey CN. RSEM: accurate transcript quantification from RNA-Seq data with or without a reference genome. *BMC Bioinformatics*. 2011;12:323.
31. Law CW, Chen Y, Shi W, Smyth GK. voom: Precision weights unlock linear model analysis tools for RNA-seq read counts. *Genome Biol*. 2014;15:R29.
32. Smyth GK. Linear models and empirical bayes methods for assessing differential expression in microarray experiments. *Stat Appl Genet Mol Biol*. 2004;3(1):1-25. <https://doi.org/10.2202/1544-6115.1027>
33. Subramanian A, Tamayo P, Mootha VK, et al. Gene set enrichment analysis: a knowledge-based approach for interpreting genome-wide expression profiles. *Proc Natl Acad Sci USA*. 2005;102:15545-15550.
34. Liberzon A, Subramanian A, Pinchback R, Thorvaldsdóttir H, Tamayo P, Mesirov JP. Molecular signatures database (MSigDB) 3.0. *Bioinformatics*. 2011;27:1739-1740.
35. Robinson JT, Thorvaldsdóttir H, Winckler W, et al. Integrative genomics viewer. *Nat Biotechnol*. 2011;29:24-26. <https://doi.org/10.1038/nbt.1754>. PMID: 21221095; PMCID: PMC3346182.
36. Bradford MM. A rapid and sensitive method for the quantitation of microgram quantities of protein utilizing the principle of protein-dye binding. *Anal Biochem*. 1976;72:248-254.
37. Smith PK, Krohn RI, Hermanson GT, et al. Measurement of protein using bicinchoninic acid. *Anal Biochem*. 1985;150:76-85.
38. Johnson VG, Mather IH. Monoclonal antibodies prepared against PAS-I, butyrophilin and GP-55 from guinea-pig milk-fat-globule membrane bind specifically to the apical pole of secretory-epithelial cells in lactating mammary tissue. *Exp Cell Res*. 1985;158:144-158.
39. Duan WR, Garner DS, Williams SD, Funckes-Shippy CL, Spath IS, Blomme EAG. Comparison of immunohistochemistry for activated caspase-3 and cleaved cytokeratin 18 with the TUNEL method for quantification of apoptosis in histological sections of PC-3 subcutaneous xenografts. *J Pathol*. 2003;199:221-228.
40. Schere-Levy C, Buggiano V, Quaglino A, et al. Leukemia inhibitory factor induces apoptosis of the mammary epithelial cells and participates in mouse mammary gland involution. *Exp Cell Res*. 2003;282:35-47.
41. Kritikou EA, Sharkey A, Abell K, et al. A dual, non-redundant, role for LIF as a regulator of development and STAT3-mediated cell death in mammary gland. *Development*. 2003;130:3459-3468.
42. Cui Y, Riedlinger G, Miyoshi K, et al. Inactivation of Stat5 in mouse mammary epithelium during pregnancy reveals distinct functions in cell proliferation, survival, and differentiation. *Mol Cell Biol*. 2004;24:8037-8047.
43. Kreuzaler PA, Staniszewska AD, Li W, et al. Stat3 controls lysosomal-mediated cell death in vivo. *Nature Cell Biol*. 2011;13:303-309.
44. Ohkawa H, Ohishi N, Yagi K. Assay for lipid peroxides in animal tissues by thiobarbituric acid reaction. *Anal Biochem*. 1979;95:351-358.
45. Conrad CC, Talent JM, Malakowsky CA, Gracy RW. Post-electrophoretic identification of oxidized proteins. *Biol Proced Online*. 1999;2:39-45.
46. Greenacre SAB, Ischiropoulos H. Tyrosine nitration: Localisation, quantification, consequences for protein function and signal transduction. *Free Radical Res*. 2001;34:541-581. <https://doi.org/10.1080/10715760100300471>
47. Gerdes J, Lemke H, Baisch H, Wacker HH, Schwab U, Stein H. Cell cycle analysis of a cell proliferation-associated human nuclear antigen defined by the monoclonal antibody Ki-67. *J Immunol*. 1984;133:1710-1715.
48. Watson CJ. Key stages in mammary gland development - Involution: apoptosis and tissue remodelling that convert the mammary gland from milk factory to a quiescent organ. *Breast Cancer Res*. 2006;8:203. <https://doi.org/10.1186/bcr1401>

49. Lund LR, Romer J, Thomasset N, et al. Two distinct phases of apoptosis in mammary gland involution: proteinase-independent and -dependent pathways. *Development*. 1996;122:181-193.
50. Li M, Liu X, Robinson G, et al. Mammary-derived signals activate programmed cell death during the first stage of mammary gland involution. *Proc Natl Acad Sci USA*. 1997;94:3425-3430.
51. Clarkson RWE, Wayland MT, Lee J, Freeman T, Watson CJ. Gene expression profiling of mammary gland development reveals putative roles for death receptors and immune mediators in post-lactational regression. *Breast Cancer Res*. 2004;6:R92-R109.
52. Stein T, Morris JS, Davies CR, et al. Involution of the mouse mammary gland is associated with an immune cascade and an acute-phase response, involving LBP, CD14 and STAT3. *Breast Cancer Res*. 2004;6:R75-R91.
53. Hughes K, Watson CJ. The multifaceted role of STAT3 in mammary gland involution and breast cancer. *Int J Mol Sci*. 2018;19(6):1695. <https://doi.org/10.3390/ijms19061695>
54. Wärrri A, Cook KL, Hu R, et al. Autophagy and unfolded protein response (UPR) regulate mammary gland involution by restraining apoptosis-driven irreversible changes. *Cell Death and Discovery*. 2018;4:40.
55. Teplova I, Lozy F, Price S, et al. ATG proteins mediate efferocytosis and suppress inflammation in mammary involution. *Autophagy*. 2013;9:459-475.
56. Monks J, Rosner D, Geske FJ, et al. Epithelial cells as phagocytes: apoptotic epithelial cells are engulfed by mammary alveolar epithelial cells and repress inflammatory mediator release. *Cell Death Diff*. 2005;12:107-114.
57. Chapman RS, Lourenco PC, Tonner E, et al. Suppression of epithelial apoptosis and delayed mammary gland involution in mice with a conditional knockout of Stat3. *Genes Develop*. 1999;13:2604-2616.
58. Yang Y-A, Tang B, Robinson G, et al. Smad3 in the mammary epithelium has a nonredundant role in the induction of apoptosis, but not in the regulation of proliferation or differentiation by transforming growth factor-beta. *Cell Growth Diff*. 2002;13:123-130.
59. Remy I, Montmarquette A, Michnick SW. PKB/Akt modulates TGF- $\beta$  signalling through a direct interaction with Smad3. *Nature Cell Biol*. 2004;6:358-365.
60. Melino G, Knight RA, Nicotera P. How many ways to die? How many different models of cell death? *Cell Death Diff*. 2005;12:1457-1462.
61. Baxter FO, Neoh K, Tevendale MC. The beginning of the end: death signaling in early involution. *J Mamm Gland Biol Neopl*. 2007;12:3-13.
62. Abell K, Bilancio A, Clarkson RWE, et al. Stat3-induced apoptosis requires a molecular switch in PI(3)K subunit composition. *Nature Cell Biol*. 2005;7:392-398.
63. Tiffen PG, Omidvar N, Marquez-Almuina N, Croston D, Watson CJ, Clarkson RWE. A dual role for oncostatin M signaling in the differentiation and death of mammary epithelial cells in vivo. *Mol Endocrinol*. 2008;22:2677-2688.
64. Reinhardt TA, Lippolis JD. Mammary gland involution is associated with rapid down regulation of major mammary Ca<sup>2+</sup>-ATPases. *Biochem Biophys Res Commun*. 2009;378:99-102.
65. VanHouten J, Sullivan C, Bazinet C, et al. PMCA2 regulates apoptosis during mammary gland involution and predicts outcome in breast cancer. *Proc Natl Acad Sci USA*. 2010;107:11405-11410.
66. Jeong J, Kim W, Hens J, et al. NHERF1 Is required for localization of PMCA2 and suppression of early involution in the female lactating mammary gland. *Endocrinology*. 2019;160:1797-1810.
67. Butturini E, Carcereri de Prati A, Mariotto S. Redox regulation of STAT1 and STAT3 signaling. *Int J Mol Sci*. 2020;21:7034. <https://doi.org/10.3390/ijms21197034>
68. Zhao L, Melenhorst JJ, Hennighausen L. Loss of interleukin 6 results in delayed mammary gland involution: a possible role for mitogen-activated protein kinase and not signal transducer and activator of transcription 3. *Mol Endocrinol*. 2002;16:2902-2912.
69. Conery AR, Cao Y, Thompson EA, Townsend CM Jr, Ko TC, Luo K. Akt interacts directly with Smad3 to regulate the sensitivity to TGF- $\beta$ -induced apoptosis. *Nature Cell Biol*. 2004;6:366-372.
70. Thangaraju M, Rudelius M, Bierie B, et al. C/EBPdelta is a crucial regulator of pro-apoptotic gene expression during mammary gland involution. *Development*. 2005;132:4675-4685.
71. Sargeant TJ, Lloyd-Lewis B, Resemann HK, Ramos-Montoya A, Skepper J, Watson CJ. Stat3 controls cell death during mammary gland involution by regulating uptake of milk fat globules and lysosomal membrane permeabilization. *Nature Cell Biol*. 2014;16:1057-1068.
72. Baxter FO, Came PJ, Abell K, et al. IKKbeta/2 induces TWEAK and apoptosis in mammary epithelial cells. *Development*. 2006;133:3485-3494.
73. Coothankandaswamy V, Elangovan S, Singh N, Prasad PD, Thangaraju M, Ganapathy V. The plasma membrane transporter SLC5A8 suppresses tumour progression through depletion of survivin without involving its transport function. *Biochem J*. 2013;450:169-178.
74. Wang H, Holloway MP, Ma L, et al. Acetylation directs survivin nuclear localization to repress STAT3 oncogenic activity. *J Biol Chem*. 2010;285:36129-36137.
75. Hughes K, Wickenden JA, Allen JE, Watson CJ. Conditional deletion of Stat3 in mammary epithelium impairs the acute phase response and modulates immune cell numbers during post-lactational regression. *J Pathol*. 2012;227:106-117.
76. Hadsell DL, Torres D, George J, Capuco AV, Ellis SE, Fiorotto ML. Changes in secretory cell turnover, and mitochondrial oxidative damage in the mouse mammary gland during a single prolonged lactation cycle suggest the possibility of accelerated cellular aging. *Exp Gerontol*. 2006;41:271-281.
77. Visvader JE, Clevers H. Tissue-specific designs of stem cell hierarchies. *Nature Cell Biol*. 2016;18:349-355.
78. Rios AC, Fu NY, Jamieson PR, et al. Essential role for a novel population of binucleated mammary epithelial cells in lactation. *Nature Commun*. 2016;7:11400.
79. Carli JFM, Trahan GD, Jones KL, et al. Single cell RNA sequencing of human milk-derived cells reveals sub-populations of mammary epithelial cells with molecular signatures of progenitor and mature states: a novel, non-invasive framework for investigating human lactation physiology. *J Mammary Gland Biol Neopl*. 2020;25(4):367-387. <https://doi.org/10.1007/s10911-020-09466-z>
80. Neifert MR. Prevention of breast feeding tragedies. *Pediatr Clinics North Amer*. 2001;48:273-297.
81. Bardanzellu F, Puddu M, Peroni DG, Fanos V. The human breast milk metabolome in overweight and obese mothers. *Front Immunol*. 2020;11:1533. <https://doi.org/10.3389/fimmu.2020.01533>
82. Isganaitis E, Venditti S, Matthews TJ, Lerin C, Demerath EW, Fields DA. Maternal obesity and the human milk metabolome: associations with infant body composition and postnatal weight gain. *Am J Clin Nutr*. 2019;110:111-120.

83. Vorbach C, Harrison R, Capecchi MR. Xanthine oxidoreductase is central to the evolution and function of the innate immune system. *Trends Immunol.* 2003;24:512-517.
84. Smith IA, Knezevic BR, Ammann JU, et al. BTN1A1, the mammary gland butyrophilin, and BTN2A2, are both inhibitors of T-cell activation. *J Immunol.* 2010;184:3514-3525.
85. Katz Y, Wang ET, Silterra J, et al. Quantitative visualization of alternative exon expression from RNA-seq data. *Bioinformatics.* 2015;31:2400-2402.
86. Banghart LR, Chamberlain CW, Velarde J, et al. Butyrophilin is expressed in mammary epithelial cells from a single-sized messenger RNA as a type I membrane glycoprotein. *J Biol Chem.* 1998;273:4171-4179.
87. Heid H, Zimbelmann R, Dörflinger Y, Rickelt S. Formation and degradation of lipid droplets in human adipocytes and the expression of aldehyde oxidase (AOX). *Cell Tiss Res.* 2020;379:45-62.

## SUPPORTING INFORMATION

Additional Supporting Information may be found online in the Supporting Information section.

**How to cite this article:** Jeong J, Kadegowda AKG, Meyer TJ, et al. The butyrophilin 1a1 knockout mouse revisited: Ablation of *Btn1a1* leads to concurrent cell death and renewal in the mammary epithelium during lactation. *FASEB BioAdvances.* 2021;3:971–997. <https://doi.org/10.1096/fba.2021-00059>

## APPENDIX

Traces of *Btn1a1* mRNA in *Btn1a1*<sup>-/-</sup> mice were confirmed by qRT-PCR RNA using primer pairs (Table S3) encompassing the area within and adjacent to the region

disrupted by the insertion of *neo*.<sup>13</sup> Message was detected that amounted to  $1.68 \pm 0.55\%$  of wild type levels for exon 4, and  $3.11 \pm 0.36\%$  for a region within exon 8, values in good agreement with the RNAseq data (–43.2-fold,

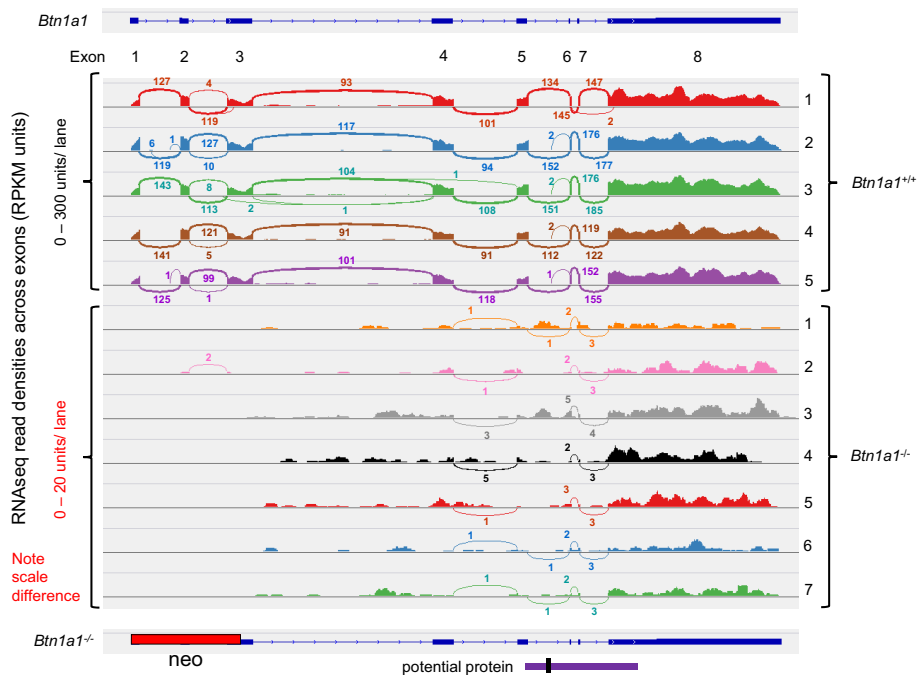


**FIGURE A1** Low levels of mRNAs encoding truncated *Btn1a1* are expressed in *Btn1a1*<sup>-/-</sup> mice. Shashimi plots of *Btn1a1* mRNAs detected by RNAseq. Transcripts from five *Btn1a1*<sup>+/+</sup> and seven *Btn1a1*<sup>-/-</sup> mice are shown from top to bottom, as indicated and the *Btn1a1* gene structure is given as a reference above the figure. Note the difference in scales between genotypes (y axis) and the limited number of partial transcripts in the knockout, compared to full-length mRNA in the wild type samples. The disrupted *Btn1a1*<sup>-/-</sup> gene structure is given below the figure and shows the position of the 3' region of the inserted neo cassette (red), which extends into the 5' region of the putative promoter of the wild type gene (not shown). Any theoretical undergraded protein in the knockout would be encoded by mRNA from the 5' region of exon 4 through the 3' end of exon 8 (purple horizontal bar) and include the transmembrane domain (vertical black bar)

2.3%). No message was detected within the ablated region encompassing exons 1 and 2. Sashimi analysis<sup>85</sup> of the RNAseq data revealed only single full-length transcripts in wild type samples, as predicted from previous work,<sup>86</sup> but truncated messages (2%–4% of wild type) in the *Btn1a1*<sup>-/-</sup> mice. These latter heterogeneous messages encompassed portions of intron 3 to the 3' end of the full-length mRNA, with the majority enveloping exon 8 and the 3' untranslated region (Figure A1). Although heterogeneous in nature, some of these molecules may be stabilized by TD-43, an RNA-binding protein, which regulates post-transcriptional stability of *Btn1a1* and *Xdh* mRNAs in wild type cells.<sup>18</sup>

Synthesis of these minor transcripts may be controlled from a downstream promoter-like region in the 3'-end

of intron 3 (Figure A2A). Several methionine start sites are in-frame close to the 5' junction of exon 4 and one is within the context of an optimal Kozak sequence (denoted in green, Figure A2A). Translation from one or more of these methionine start sites would generate protein fragments comprising the IgC1 fold in the exoplasmic domain, the membrane anchor and the entire cytoplasmic region. In the absence of the N-terminal signal sequence encoded by exon 2, most of this potential membrane protein is predicted to misfold in the cytoplasm and be degraded.

We found no evidence for a truncated fragment with a predicted Mr of approx. 50,000 by immunoblot of tissue fractions (Figure A3A,B,D) using an anti-peptide antibody to the C-terminus of *Btn1a1*.<sup>13</sup> However, an immunoreactive band of protein with an approx. Mr of 150,000 was



**FIGURE A2** Potential origin and analysis of truncated *Btn1a1* protein synthesized in *Btn1a1*<sup>-/-</sup> mice. (A) Sequence of putative downstream promoter in the 3'-region of intron 3 (grey shading) and adjoining sequence of exon 4. Potential transcription factor binding sites shown in the intron include those for PPAR proteins (yellow), Stat factors (white), Sp1 (light blue), and GR half sites (dark blue). An imperfect TATA box (orange) lies just 5' of the contiguous exon and in-frame ATG start sites (red). One ATG start site shown in green is within an optimal Kozak consensus sequence. The potential N-terminal M residues of any translated protein are shown in the primary sequence below the gene structure using the same red and green color code as in the ATG codons in the gene sequence. (B) Peptides identified by GC-mass spectrometry in (PNS) samples from *Btn1a1*<sup>+/+</sup> and *Btn1a1*<sup>-/-</sup> mice. Peptides are color-coded in the sequence on the left and Table on the right. Theoretical N-terminus of protein encoded by truncated mRNA (arrow), optimal M translational start site (circle), transmembrane domain (italicized letters, black underline), essential Xdh binding site (purple underline), sequence used for anti-peptide antibody (dashed black line)

detected in THs from all three genotypes that was most abundant in *Btn1a1*<sup>-/-</sup> samples (arrowhead, Figure A3B). This pattern of immunostaining mirrored that for Xdh on the same blot, which had been stripped and reprobed with an antibody to the C-terminus of mouse Xdh<sup>7</sup> (Figure A3C). This concordance was consistently noted in at least five similar blots with 90 samples separated in either 6 or 10% acrylamide gels.

*Btn1a1*, identified by mass spectrometric analysis, binds to Xdh in blots of human milk-fat-globule membrane separated under reducing conditions,<sup>87</sup> presumably because of tight binding between the two proteins.<sup>7</sup> Thus, it is possible that truncated nascent *Btn1a1* protein may bind through its C-terminus<sup>7</sup> to Xdh in the cytoplasm before the bulk of exposed misfolded *Btn1a1* is degraded in the proteasome. In this event, C-terminal epitopes of *Btn1a1*

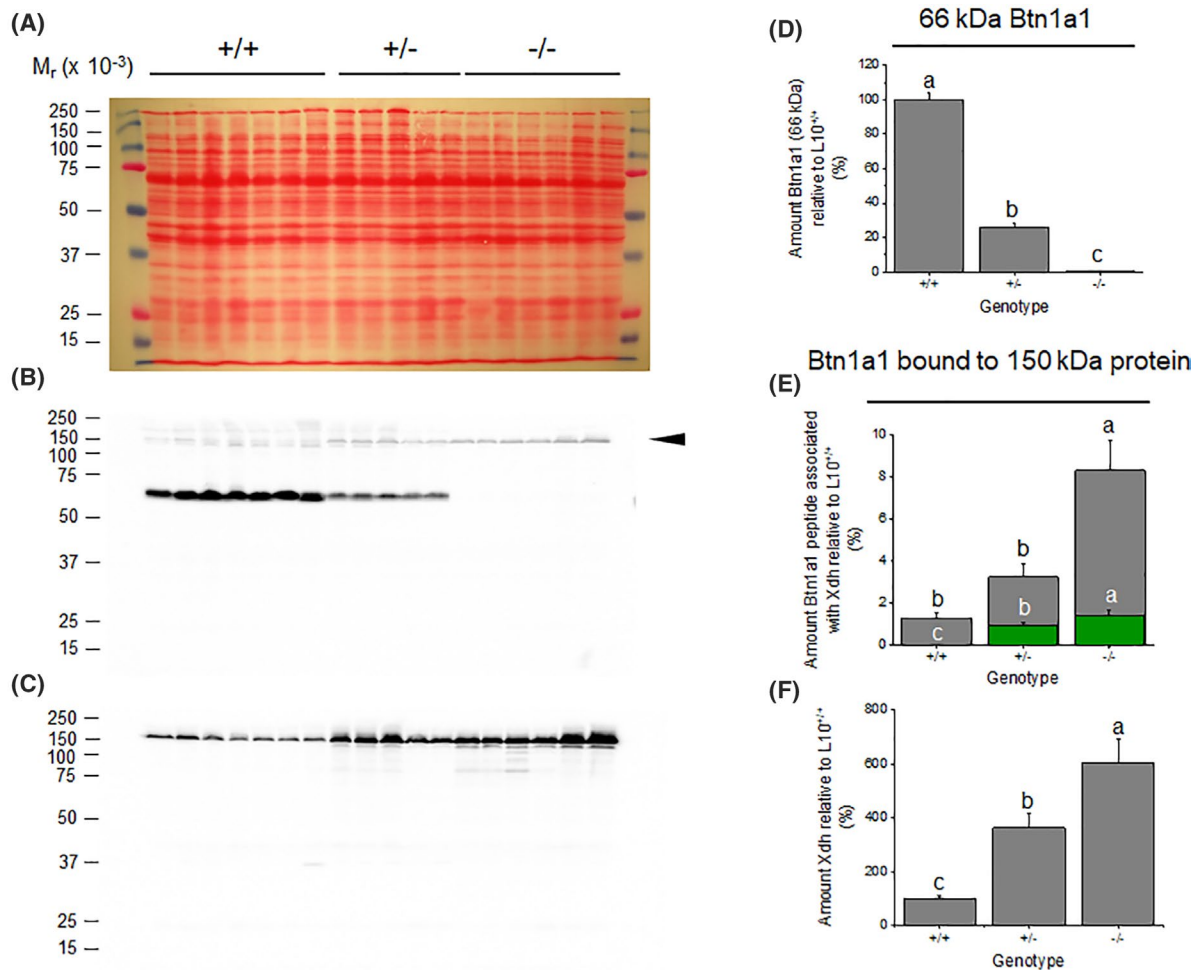


**FIGURE A3** Determination of the amounts of Btn1a1 and Xdh in the lactating mammary glands of *Btn1a1*<sup>+/+</sup>, *Btn1a1*<sup>+/-</sup>, and *Btn1a1*<sup>-/-</sup> mice by immunoblot. A-C. THs of mammary tissue, at days 9–11 of lactation, from seven *Btn1a1*<sup>+/+</sup>, five *Btn1a1*<sup>+/-</sup>, and six *Btn1a1*<sup>-/-</sup> mice and *M<sub>r</sub>*-marker proteins were separated by SDS–polyacrylamide gel electrophoresis (75 μg protein/lane; 10% polyacrylamide) and electroblotted to nitrocellulose. (A) Ponceau-S stained blot. (B) Btn1a1 detected with a 5000-fold dilution of rabbit anti-peptide antibody to mouse Btn1a1 (Table S1), followed by a 3000-fold dilution of goat anti-rabbit IgG-HRP conjugate. Exposure was under nonlinear conditions to reveal the minor amounts of immunoreactive peptide bound to the 150 kDa-band of Xdh in the *Btn1a1*<sup>-/-</sup> samples (arrowhead). (C) Xdh detected in the same stripped blot with a 5000-fold dilution of rabbit anti-peptide antibody to mouse Xdh (Table S1), followed by a 3,000-fold dilution of goat anti-rabbit IgG-HRP conjugate. (D–F) Quantitation of the amounts of Btn1a1 and Xdh in triplicate blots under non-saturating conditions. (D, E) Relative amounts of Btn1a1, viz, D the major 66 kDa-band of Btn1a1 in B, and E, the Btn1a1 peptide bound to Xdh (arrowhead in B), normalized to the 66 kDa-band in the *Btn1a1*<sup>+/+</sup> samples, set as 100%. Green columns show the same data corrected for the increases of Xdh noted in F below. See text for further discussion. (F) Amounts of Xdh in the same blots used for Btn1a1 analysis, stripped of residual antibodies, and normalized to *Btn1a1*<sup>+/+</sup> (set as 100%). There was a 3.6-fold increase of Xdh in *Btn1a1*<sup>+/-</sup> samples, and a sixfold increase in *Btn1a1*<sup>-/-</sup> samples compared with the amount in *Btn1a1*<sup>+/+</sup> mice. Columns with different letters are statistically different from each other. Means ± SEM, p < 0.05, F-test (ANOVA)

would be protected and recognized by the C-terminal anti-peptide antibody used for the immunoblots. Furthermore, the C-terminal region of Btn1a1 bound to Xdh will be selectively enriched with the increased amounts of Xdh in knockout samples (an approx. sixfold increase in Xdh over wild type levels, Figures 1C, A3F, Table S4). Taking this sixfold enrichment into account, the C-terminal epitopes identified in knockout samples account for approx. 1.5% of wild type values (green bars, Figure A3E, Table S4).

Eight peptides of Btn1a1 protein were detected in wild type and three in knockout samples by LC-mass spectrometry (Figure A2B) with overall decreases in amount (null/wild type) of fivefold by pair-wise and 22-fold by simple arithmetic ratios (Excel Spreadsheets 1,3). Btn1a1 peptide was not detected in the ablated and adjoining N-terminal region (peptides 1-3). However, there were significant amounts of two peptides, on either

side of the membrane anchor (peptides 4-5), within the region encoded by the 5' end of the truncated mRNA identified by Sashimi analysis. The most abundant peptide (peptide 5) lies within the N-terminal region of the B30.2 domain but this peptide was the most variable in amount. Further downstream toward the C-terminus only one of the three peptides (peptide 7) was detected in the knockout samples, albeit at low levels (3% of wild type). Most importantly, this latter peptide encompasses the region essential for binding to Xdh (purple underline, Figure A2B).<sup>7</sup> Thus, although Btn1a1 protein is synthesized from a truncated message, the bulk of it is degraded, including most of the B30.2 domain and the C-terminal region. However, epitopes within the terminal 21 amino acids may be protected by binding to Xdh, and therefore are detected on immunoblots (arrow, Figure A3B).